PTEP

Preprint number: KUNS2618

Possible relevance of the softening of the sigma meson to η decay into 3π in the nuclear medium

Shuntaro Sakai and Teiji Kunihiro

Department of Physics, Kyoto University, Kitashirakawa-Oiwakecho, Kyoto 606-8502, Japan
**E-mail: s.sakai@ruby.kyoto-u.ac.jp*

arXiv:1512.04000v2 [nucl-th] 20 Jun 2016

We investigate the role of the softening of the scalar−isoscalar (sigma) meson in the $\eta \to \pi^+\pi^-\pi^0$ and $3\pi^0$ decay widths in the symmetric nuclear medium using a linear sigma model. Our calculation shows that these decay widths in the nuclear medium increase by up to a factor of four to ten compared with those in the free space mainly depending on the mass of the sigma meson in the free space which is an input parameter of the model. The enhancements are considerable even at a half of the normal nuclear density. Thus, the η decay into 3π could be a possible new probe for the chiral restoration in the nuclear medium. We find that the density dependence of the $\eta \to 3\pi^0$ decay is moderate in comparison with that of $\eta \to \pi^+\pi^-\pi^0$, although the former width is greater than the latter one at a given density: This is because the softening of the sigma meson causes cancellation of the terms appearing from the Bose symmetry in the $\eta \to 3\pi^0$ decay. The difference between the density dependences should be helpful for experimental confirmation of the findings of the present study.

Subject Index xxxx, xxx

1. Introduction

The $\eta \to 3\pi$ decay process[1] is prohibited by G parity conservation, which, conversely, implies that the isospin-symmetry breaking (ISB) can cause the process. The possible sources of ISB are the electromagnetic interaction and the tiny mass difference of the u and d quarks from the viewpoint of quantum chromodynamics. Studies using the current-algebra technique [1–4], however, revealed that their leading-order contributions give a far smaller value of the decay width than the experimental one. The smallness of the higher-order contributions from the electromagnetic effect is confirmed in Refs. [5, 6]. There have been many investigations based on the strong interaction [7–13][2] because it should be responsible for the discrepancy of the decay widths between the experimental value and the current-algebra estimation. In addition to ISB, the significant effect of the final-state interaction (FSI) was pointed out in Refs. [16, 17]; see Refs. [18–25] for later studies on this subject.

The modification of hadron properties in the nuclear medium is an interesting topic in hadron physics. A focus of the study is to investigate chiral restoration in the nuclear medium (see, e.g., Ref. [26] for a summary of the theoretical and experimental status); the chiral restoration means the reduction of the quark condensate which is the order parameter of the spontaneous breaking of chiral symmetry, in the environment (e.g., a heat bath or hadronic matter).

In the previous study [27], the present authors investigated the $\eta \to 3\pi$ decay width in the asymmetric nuclear medium, anticipating that the external isospin asymmetry would enhance the decay width; the isospin symmetry is explicitly broken by the asymmetric nuclear density $\delta\rho = \rho_n - \rho_p \neq 0$ besides the mass difference of the u and d quarks, where ρ_p and ρ_n are the proton and neutron number densities, respectively. The analysis is based on a nonlinear sigma model. The effect of FSI in the $I = J = 0$ channel, i.e. the sigma-meson channel is included within the meson one-loop diagrams [18, 23]. Then, the decay width in the free space shows a fairly good agreement with the experimental value and the remaining minor effects may be accounted for by a more complete treatment of FSI, such as the incorporation of the ρ meson contribution in the t-channel. It was found that the $\eta \to 3\pi$ decay width is enhanced as the total baryon density $\rho = \rho_n + \rho_p$ as well as $\delta\rho$ increases. In the enhancement of the decay width by ρ, the 4-meson–N–N vertex, which is active only in the nuclear medium, gives a significant contribution, as in the enhancement of the in-medium $\pi\pi$ cross section in the $I = J = 0$ channel [28]. The 4π–N–N vertex is traced back to the contribution from the scalar meson in the linear representation [29]. Then, we expect that the enhancement of the $\eta \to 3\pi$ decay width is also associated with the dynamics of the scalar meson in the nuclear medium.

The nature of light scalar mesons has attracted much attention in recent years; the observed resonance in the $\pi\pi$ ($I = J = 0$) channel (see, e.g., the section "Note on scalar meson below 2 GeV" in Ref. [30] for a summary of the current status) may be a hadronic molecule of 2π [31], a tetraquark meson [32], or a light scalar glueball [33]. In addition, it can be a quantum fluctuation of the order parameter associated with the spontaneous breaking of the chiral symmetry [34–36]. The observed scalar meson would be a superposition of the

[1] We denote the decay processes $\eta \to \pi^+\pi^-\pi^0$ and $3\pi^0$ by $\eta \to 3\pi$ for short.

[2] Works involving the scalar meson, which had been previously reported in, e.g., Ref. [14], are summarized in Ref. [15].

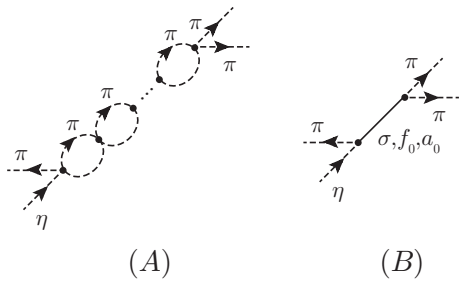

Fig. 1 A schematic figure showing the FSI of pions. The solid and dashed lines indicate the scalar and pseudoscalar mesons. In this study, we assume that the contribution from the poles of the scalar mesons given in diagram (B) can be substituted for the effect of the FSI of pions represented as diagram (A).

aforementioned states. For the scalar meson in LσM which is the fluctuation mode of the order parameter and is called the sigma meson in the following, it is anticipated to be softened through chiral restoration [36–40]. Recalling that FSI in the sigma-meson channel makes a significant contribution, we expect that the $\eta \to 3\pi$ decay width is enhanced in association with the softening of the sigma meson, and thereby the chiral restoration in the nuclear medium can be probed through the decay process.

In this study, we investigate the $\eta \to 3\pi$ decay width in the symmetric nuclear medium using LσM, focusing on the softening of the sigma meson. Within LσM, the softening of the sigma meson is automatically built in. As alluded to above, the formation of the resonance is responsible for FSI in the $\pi\pi$ $(I = J = 0)$ channel; see Fig. 1 for a schematic figure of FSI, where the ρ meson contribution in the $\pi\pi$ $(I = 1)$ channel is ignored in the expectation that the contribution is small because its pole position is far from the kinematically allowed region of the Dalitz plot of the $\eta \to 3\pi$ decay. The in-medium modification of the ρ meson properties, e.g., the mass reduction [41] or the broadening of the width [42], would affect the $\eta \to 3\pi$ decay in the nuclear medium, though its contribution will be ignored, as stated above: The modification of the ρ meson properties in the nuclear medium would also be small because our calculation is limited to the small densities, as will be clarified in the following section. Thus, the effect from the ρ meson in the nuclear medium would be small in the situation treated in the present work.

It is known that the couplings with excited baryons, e.g. $N^*(1535)$, have interesting effects on the in-medium properties of the η or π mesons (see, e.g., Ref. [43]). These are not taken into account in the present work either, to allow us to focus on the role of the softening of the sigma meson in the $\eta \to 3\pi$ decay. The inclusion of these effects will be left for future work.

In the present paper, we shall show an enhancement of the $\eta \to 3\pi$ decay width in the nuclear medium. The decay width becomes about four to ten times larger than the value in the free space depending on the mass of the sigma meson in the free space, which is an input parameter of our calculation. The mechanism of the resultant enhancement is found to be similar to that of the $\pi\pi(I = J = 0)$ cross section in the nuclear medium [29], where the growth of the spectral function in the sigma channel near the 2π threshold plays an essential role. The enhancement of the decay width is considerable even at small densities;

indeed, the decay width at half of the normal nuclear density is several times larger than that in the free space.

We find that the enhancement of the $\eta \to 3\pi^0$ decay width in the nuclear medium is weaker than that of the $\eta \to \pi^+\pi^-\pi^0$ decay at large ρ though the decay width of $\eta \to 3\pi^0$ itself is larger than that of $\eta \to \pi^+\pi^-\pi^0$. We shall show that this is because some of the terms appearing from the Bose symmetry of $3\pi^0$ cancel each other when the mass of the sigma meson approaches the 2π threshold.

This paper is constructed as follows. In Sect. 2, we introduce the setup of our model. In the subsequent section, we explain the method used to include the effect of the nuclear medium. Then in Sect. 4, we present the numerical results of the decay widths of the η meson into $\pi^+\pi^-\pi^0$ and $3\pi^0$ with some discussions. Finally, we give a summary and some remarks in Sect. 5. Some details of our calculation are presented in the appendices.

2. Model

In this section, we introduce the model used in our calculation.

The meson and baryon fields belong to the $(\mathbf{3}_L, \bar{\mathbf{3}}_R) \oplus (\bar{\mathbf{3}}_L, \mathbf{3}_R)$ representation of the chiral SU(3) group. The meson (baryon) field $M(B)$ is transformed into $LM(B)R^\dagger$ under the chiral SU(3) transformation, where L, R are elements of SU(3). For the baryon field, we omit the hyperons which do not appear in this calculation.

The Lagrangian of LσM used in this study is given as follows:

$$\begin{aligned}\mathcal{L} =& \frac{1}{2}\mathrm{tr}(\partial_\mu M \partial^\mu M^\dagger) - \frac{\mu^2}{2}\mathrm{tr}(MM^\dagger) - \frac{\lambda}{4}\mathrm{tr}(MM^\dagger)^2 - \frac{\lambda'}{4}[\mathrm{tr}(MM^\dagger)]^2 + \frac{B}{2}(\det M + \det M^\dagger) \\ &+ \frac{A}{2}\mathrm{tr}(\chi M^\dagger + M\chi^\dagger) + \bar{N}\left(i\partial\!\!\!/ - gM_5\right)N, \end{aligned} \tag{1}$$

$$M = M_s + iM_{ps} = \sum_{a=0}^{8}\frac{\lambda_a \sigma_a}{\sqrt{2}} + i\sum_{a=0}^{8}\frac{\lambda_a \pi_a}{\sqrt{2}},\ N = {}^t(p, n),\ \chi = \mathrm{diag}(m_u, m_d, m_s), \tag{2}$$

$$M_s = \begin{pmatrix} \sigma_u & a_0^+ & \kappa^+ \\ a_0^- & \sigma_d & \kappa^0 \\ \kappa^- & \bar{\kappa}^0 & \sigma_s \end{pmatrix}, \tag{3}$$

$$M_{ps} = \begin{pmatrix} \eta_0/\sqrt{3} + \pi_3/\sqrt{2} + \eta_8/\sqrt{6} & \pi^+ & K^+ \\ \pi^- & \eta_0/\sqrt{3} - \pi_3/\sqrt{2} + \eta_8/\sqrt{6} & K^0 \\ K^- & \bar{K}^0 & \eta_0/\sqrt{3} - 2\eta_8/\sqrt{6} \end{pmatrix}, \tag{4}$$

$$M_5 = \begin{pmatrix} \sigma_u & & \\ & \sigma_d & \end{pmatrix} + i\gamma_5 \begin{pmatrix} \frac{\eta_0}{\sqrt{3}} + \frac{\pi_3}{\sqrt{2}} + \frac{\eta_8}{\sqrt{6}} & & \\ & \frac{\eta_0}{\sqrt{3}} - \frac{\pi_3}{\sqrt{2}} + \frac{\eta_8}{\sqrt{6}} & \end{pmatrix}, \tag{5}$$

$$\sigma_u = \frac{\sigma_0}{\sqrt{3}} + \frac{\sigma_3}{\sqrt{2}} + \frac{\sigma_8}{\sqrt{6}},\ \sigma_d = \frac{\sigma_0}{\sqrt{3}} - \frac{\sigma_3}{\sqrt{2}} + \frac{\sigma_8}{\sqrt{6}},\ \sigma_s = \frac{\sigma_0}{\sqrt{3}} - \frac{2}{\sqrt{6}}\sigma_8. \tag{6}$$

Here, λ^a is the Gell-Mann matrix with the normalization $\mathrm{tr}(\lambda^a\lambda^b) = 2\delta^{ab}$.

The tree-level effective potential of the scalar fields in the nuclear medium $V_{\mathrm{eff}}(\sigma_u, \sigma_d, \sigma_s; \rho)$ and the conditions to determine their expectation values are given as follows;

$$\begin{aligned} V_{\mathrm{eff}}(\sigma_u, \sigma_d, \sigma_s; \rho) =& \frac{\mu^2}{2}(\sigma_u^2 + \sigma_d^2 + \sigma_s^2) + \frac{\lambda}{4}(\sigma_u^4 + \sigma_d^4 + \sigma_s^4) + \frac{\lambda'}{4}(\sigma_u^2 + \sigma_d^2 + \sigma_s^2)^2 \\ &- B\sigma_u\sigma_d\sigma_s - A(m_u\sigma_u + m_d\sigma_d + m_s\sigma_s) + g(\rho_p + \rho_n), \end{aligned} \tag{7}$$

$$\frac{\partial V_{\rm eff}}{\partial \sigma_u} =\mu^2\sigma_u + \lambda\sigma_u^3 + \lambda'\sigma_u(\sigma_u^2+\sigma_d^2+\sigma_s^2) - B\sigma_d\sigma_s - Am_u + g\rho_p = 0, \tag{8}$$

$$\frac{\partial V_{\rm eff}}{\partial \sigma_d} =\mu^2\sigma_d + \lambda\sigma_d^3 + \lambda'\sigma_d(\sigma_u^2+\sigma_d^2+\sigma_s^2) - B\sigma_u\sigma_s - Am_d + g\rho_n = 0, \tag{9}$$

$$\frac{\partial V_{\rm eff}}{\partial \sigma_s} =\mu^2\sigma_s + \lambda\sigma_s^3 + \lambda'\sigma_s(\sigma_u^2+\sigma_d^2+\sigma_s^2) - B\sigma_u\sigma_d - Am_s = 0. \tag{10}$$

Using the Fermi momentum of the proton (neutron) $k_f^{p(n)}$, the proton (neutron) number density is expressed as $\rho_{p(n)} = k_f^{p(n)3}/3\pi^2$. Here, we assume only the scalar fields to have the nonzero expectation values. The expectation values of the sigma fields $\langle\sigma_u\rangle$, $\langle\sigma_d\rangle$, and $\langle\sigma_s\rangle$ are determined so as to solve these equations. We keep only the terms up to $O(k_f^3)$, which corresponds to the Fermi gas approximation. Then, the contribution from the Fermi sea is omitted because it is $O(k_f^5)$ within the nonrelativistic approximation for the nucleon field. The effect of the nucleon loop in the free space is also neglected in this calculation in the expectation that the effect is suppressed by the large nucleon mass.

From the Lagrangian given by Eq. (1), the axial current A_μ^a is obtained as

$$A_\mu^a = {\rm tr}\left[\partial_\mu M_{ps}\left\{\lambda^a, M_s\right\} - \partial_\mu M_s\left\{\lambda^a, M_{ps}\right\}\right]. \tag{11}$$

Comparing this with the definition of the meson decay constants, $\left\langle 0\left|A_\mu^a(x)\right|\pi^b(p)\right\rangle = ip_\mu f_a\delta^{ab}e^{-ip\cdot x}$, those of the pion and the kaon are obtained as

$$f_{\pi^0} = f_{\pi^\pm} = \frac{\langle\sigma_u\rangle + \langle\sigma_d\rangle}{\sqrt{2}}, \tag{12}$$

$$f_{K^\pm} = \frac{\langle\sigma_u\rangle + \langle\sigma_s\rangle}{\sqrt{2}}, \tag{13}$$

$$f_{K^0} = \frac{\langle\sigma_d\rangle + \langle\sigma_s\rangle}{\sqrt{2}}, \tag{14}$$

respectively. For later convenience, we define $\sigma_q \equiv (\sigma_u+\sigma_d)/2$ and $\delta\sigma_q \equiv (\sigma_d-\sigma_u)/2$. In the isospin-symmetric limit, $\langle\sigma_u\rangle = \langle\sigma_d\rangle = \langle\sigma_q\rangle$ and $\langle\delta\sigma_q\rangle = 0$. The parameters contained in the meson part of the Lagrangian, μ^2, λ, λ', B, A, and the expectation values of the sigma fields $\langle\sigma_q\rangle$ and $\langle\sigma_s\rangle$ in the free space are determined so as to reproduce the observed meson masses and decay constants at $\rho = 0$ in the isospin-symmetric limit; explicit expressions for the meson masses are presented in Appendix A. See Ref. [44] and references therein for more details. However, it should be noted that some of the parameters in the meson sector in the present work are different from those in Ref. [44] because of the different choice of input parameters: in the present study, the parameters are determined so as to precisely reproduce the η meson mass among others. Furthermore, the sigma meson mass in the free space will be varied as an input parameter; we present the numerical results evaluated using $m_\sigma(\rho=0) = 441$, 550, and 668 MeV in Sect. 4.

The breaking of the isospin symmetry in the free space is taken into account as a small perturbation, and thus we have

$$\langle\delta\sigma_q\rangle = \frac{(m_{K^0}^2 - m_{K^\pm}^2) - (m_{\pi^0}^2 - m_{\pi^\pm}^2)}{2B + 2\lambda(2\langle\sigma_q\rangle - \langle\sigma_s\rangle)}, \tag{15}$$

where Dashen's theorem [45] has been employed to omit the leading-order correction of the pseudoscalar meson masses coming from the electromagnetic effect. We show the input

f_π	f_K	m_π	m_K	$m_{\eta'}^2 + m_\eta^2$	m_q	m_{σ_0}
92.2	110.4	138.04	495.64	$547.85^2 + 1092.0^2$	$(2.3 + 4.8)/2$	518.3, 628, 775.2

Table 1 The input values of the basic observables used for the determination of the parameters in the Lagrangian. The units of the meson decay constants and meson masses are MeV. We use the isospin average of the Particle Data Group value [30] for m_π, m_K, and m_q. The three values listed in the m_{σ_0} column are the input ones for $m_\sigma(\rho = 0) = 441$, 550, and 668 MeV.

$\langle\sigma_u\rangle$	$\langle\sigma_d\rangle$	$\langle\sigma_s\rangle$	m_u	m_d	m_s	μ^2	λ	λ'	A	B	g
64.8	65.6	90.9	2.12	4.98	106.1	2.79×10^5	45.6	-1.70	3.50×10^5	4.67×10^3	6.61

Table 2 The values of the determined parameters in the Lagrangian with $m_\sigma(\rho = 0) = 441$ MeV. The units of the parameters μ^2 and A are MeV^2, those of λ and λ' are dimensionless, and those of the others are MeV.

m_σ	m_{f_0}	$m_{a_0^0}$	$m_{a_0^\pm}$	$m_{\eta'}$	m_η	m_{π^0}	$m_{\pi^\pm}$	$m_{K^\pm}$	m_{K^0}
441	1238	1120	1120	1093	547.8	137.9	138.0	493.0	498.2

θ_s	$\theta_{a_0\sigma}$	$\theta_{a_0 f_0}$	θ_{ps}	$\theta_{\pi^0\eta}$	$\theta_{\pi^0\eta'}$	$\langle\bar{u}u\rangle$	$\langle\bar{d}d\rangle$	$\langle\bar{s}s\rangle$
13.6	-0.40	5.5×10^{-2}	-1.89	0.72	1.44×10^{-2}	-283.0^3	-284.2^3	-316.9^3

Table 3 The obtained meson masses, meson mixing angles, and quark condensate in the free space for the case of $m_\sigma(\rho = 0) = 441$ MeV. The units of the meson masses, quark condensates, and mixing angles are MeV, MeV^3, and degrees, respectively.

$\langle\sigma_u\rangle$	$\langle\sigma_d\rangle$	$\langle\sigma_s\rangle$	m_u	m_d	m_s	μ^2	λ	λ'	A	B	g
64.8	65.6	90.9	2.12	4.98	106.1	2.14×10^5	45.6	2.16	3.50×10^5	4.67×10^3	9.96

Table 4 The values of the determined parameters in the Lagrangian with $m_\sigma(\rho = 0) = 550$ MeV. The units of the parameters are the same as those in Table 2.

parameters except for the sigma meson mass in Table 1, and the determined values of the parameters in the Lagrangian are given in Tables 2, 4, and 6 for $m_\sigma(\rho = 0)$ =441, 550, and 668 MeV, respectively. The obtained meson masses and the mixing angles are presented in Tables 3, 5, and 7 for $m_\sigma(\rho = 0) = 441, 550$, and 668 MeV, respectively. The definition of the mixing angle is given in Appendix A. The parameters μ^2, λ', the masses of σ, f_0, a_0, and the mixing angles between them are changed along with $m_\sigma(\rho = 0)$.

Writing the expectation values in the free space and the nuclear medium as $\langle\ldots\rangle_0$ and $\langle\ldots\rangle_\rho$, respectively, we obtain the difference between the expectation values of the scalar meson fields $\delta\langle\sigma_i\rangle = \langle\sigma_i\rangle_\rho - \langle\sigma_i\rangle_0$ $(i = u, d, s)$ within the leading order of the baryon density ρ as follows:

$$\begin{pmatrix} \delta\langle\sigma_u\rangle \\ \delta\langle\sigma_d\rangle \\ \delta\langle\sigma_s\rangle \end{pmatrix} = -\begin{pmatrix} m_{uu}^2 & m_{ud}^2 & m_{us}^2 \\ m_{du}^2 & m_{dd}^2 & m_{ds}^2 \\ m_{su}^2 & m_{sd}^2 & m_{ss}^2 \end{pmatrix}^{-1} \begin{pmatrix} g\rho_p \\ g\rho_n \\ 0 \end{pmatrix}, \tag{16}$$

m_σ	m_{f_0}	$m_{a_0^0}$	$m_{a_0^\pm}$	$m_{\eta'}$	m_η	m_{π^0}	$m_{\pi^\pm}$	$m_{K^\pm}$	m_{K^0}
550	1247	1120	1120	1093	547.8	137.9	138.0	493.0	498.2

θ_s	$\theta_{a_0\sigma}$	$\theta_{a_0 f_0}$	θ_{ps}	$\theta_{\pi^0\eta}$	$\theta_{\pi^0\eta'}$	$\langle\bar{u}u\rangle$	$\langle\bar{d}d\rangle$	$\langle\bar{s}s\rangle$
15.7	-0.47	-4.66×10^{-2}	-1.89	0.72	1.44×10^{-2}	-283.0^3	-284.2^3	-316.9^3

Table 5 The obtained meson masses, meson mixing angles, and quark condensate in the free space for the case of $m_\sigma(\rho=0)=550$ MeV. The units of these values are the same as those in Table 3.

$\langle\sigma_u\rangle$	$\langle\sigma_d\rangle$	$\langle\sigma_s\rangle$	m_u	m_d	m_s	μ^2	λ	λ'	A	B	g
64.8	65.6	90.9	2.12	4.98	106.1	1.24×10^5	45.6	7.53	3.50×10^5	4.67×10^3	14.1

Table 6 The values of the determined parameters in the Lagrangian with $m_\sigma(\rho=0)=668$ MeV. The units of the parameters are same as those in Table 2.

m_σ	m_{f_0}	$m_{a_0^0}$	$m_{a_0^\pm}$	$m_{\eta'}$	m_η	m_{π^0}	$m_{\pi^\pm}$	$m_{K^\pm}$	m_{K^0}
668	1261	1120	1120	1093	547.8	137.9	138.0	493.0	498.2

θ_s	$\theta_{a_0\sigma}$	$\theta_{a_0 f_0}$	θ_{ps}	$\theta_{\pi^0\eta}$	$\theta_{\pi^0\eta'}$	$\langle\bar{u}u\rangle$	$\langle\bar{d}d\rangle$	$\langle\bar{s}s\rangle$
19.2	-0.6	-0.19	-1.89	0.72	1.44×10^{-2}	-283.0^3	-284.2^3	-316.9^3

Table 7 The obtained meson masses, meson mixing angles, and quark condensate in the free space for the case of $m_\sigma(\rho=0)=668$ MeV. The units of these values are the same as those in Table 3.

where $m_{ij}^2=\partial^2 V_{\rm eff}/\partial\sigma_i\partial\sigma_j$ $(i,j=u,d,s)$. Explicit expressions for m_{ij}^2 are given in Appendix A. The meson−nucleon coupling constant g in Eq. (1) is determined so as to reproduce the 30% reduction of the quark condensate at the normal nuclear density $\rho_0=0.17$ fm^{-3}, which is suggested from the analysis of the deeply bound state of the pionic atom [46].

3. Medium effect on masses and vertices of mesons

In this section, we evaluate the nuclear medium effects on the self-energies and the vertices of the mesons. Our calculation is based on the expansion with respect to the Fermi momentum k_f of the nuclear medium; we retain the terms up to $O(k_f^3)$ as mentioned in the previous section. The nucleon propagator in the nuclear medium $G(p;k_f)$ with p being the nucleon four-momentum reads

$$iG(p;k_f)=(\not{p}+m_N)\left\{\frac{i}{p^2-m_N^2+i\epsilon}-2\pi\delta(p^2-m_N^2)\theta(p_0)\theta(k_f-|\vec{p}|)\right\}, \qquad (17)$$

where the first and second terms are the contributions from the nucleon propagation in the free space and the nuclear hole state in the Fermi sea, respectively. At the leading order with respect to the Fermi momentum, the meson loops do not have the nuclear medium effect on the masses or the vertices of mesons.

The couplings of hadrons $g_{\sigma_f\sigma_1\sigma_2}, g_{\sigma_f\pi_1\pi_2}, g_{\sigma_i N}$, and $g_{\pi_i N}$ appearing in the following calculations are presented in Appendix B.

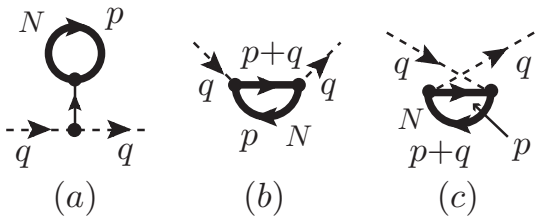

Fig. 2 Diagrams contributing to the meson self-energies in the nuclear medium. The thin and thick lines represent the propagation of the scalar meson and the nucleon, respectively. The external dashed lines represent the scalar or pseudoscalar mesons.

3.1. Medium effect on meson masses

We evaluate the nucleon one-loop diagrams shown in Fig. 2 to the meson self-energies in the nuclear medium; the leading contributions with respect to the Fermi momentum appear from these diagrams. Diagram (a) represents the contribution from the nucleon tadpole; diagrams (b) and (c) the particle−hole excitations. The self-energies of the scalar and pseudoscalar mesons in the nuclear medium $\Sigma_s(\rho)$ and $\Sigma_{ps}(\rho)$ are given as follows, respectively (see Appendix A for the details of the calculation):

$$-i\Sigma_s(\rho) = -i\frac{g_{\sigma_k N} g_{\sigma_k \sigma_1 \sigma_2}}{m_{\sigma_k}^2}\rho_{p(n)}, \tag{18}$$

$$-i\Sigma_{ps}(\rho) = -i\frac{g_{\sigma_k N} g_{\sigma_k \pi_1 \pi_2}}{m_{\sigma_k}^2}\rho_{p(n)} - i\frac{g_{\pi_1 N} g_{\pi_2 N}}{m_N}\rho_{p(n)}. \tag{19}$$

We note that the particle−hole excitations do not contribute to the self-energy of the scalar meson up to $O(k_f^3)$.

The sigma meson has a finite decay width due to the coupling with the 2π state. We implement this by the replacement of the sigma propagator $i/(p^2 - m_\sigma^2 + i\epsilon)$ with

$$iG_\sigma(p^2) = \frac{i}{p^2 - m_\sigma^2 + i\Theta(p^2)}, \tag{20}$$

where $\Theta(p^2)$ denotes the width of the sigma meson. At tree level, it reads

$$\Theta(p^2) = \frac{g_{\sigma\pi\pi}^2}{16\pi}\sqrt{1 - 4m_\pi^2/p^2}\,\theta(p^2 - 4m_\pi^2) \equiv \Theta_{\rm tree}(p^2). \tag{21}$$

Various quantum effects would modify the width from $\Theta_{\rm tree}(p^2)$ although its quantitative evaluation is beyond the scope of the present work. In the present work, we shall use $\Theta_{\rm tree}(p^2)$ as a typical width and vary $\Theta(p^2)$ within 30% around $\Theta_{\rm tree}(p^2)$ to see uncertainties of the results on the $\eta \to 3\pi$ decay width due to that of the width.

3.2. Medium effect on vertices of mesons

The modifications of the vertices of mesons come from the diagrams shown in Fig. 3. Here, we write the momenta of the outgoing meson π_i, the incoming scalar meson σ_f, and the η meson in the initial state as k_i, $\tilde{q} = k_1 + k_2$, and $q = k_1 + k_2 + k_3$, respectively. The leading corrections with respect to the Fermi momentum Γ_α and Γ_β of the scalar–2-pseudoscalar and the 4-pseudoscalar meson couplings from diagram (α) and (β) in Fig. 3 are calculated

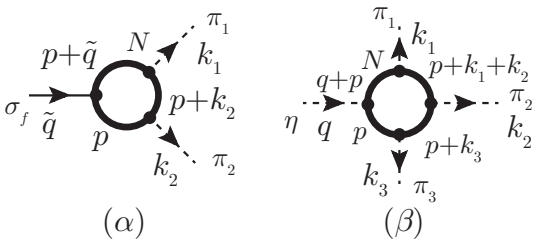

Fig. 3 Diagrams contributing to the modification of the vertices of mesons. The thin and thick solid lines denote the propagation of the scalar meson and the nucleon, and the dashed line the propagation of the pseudoscalar meson.

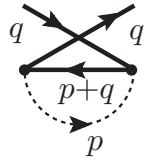

Fig. 4 Diagram contributing to the self-energy of the nucleon in the nuclear medium.

to be

$$i\Gamma_\alpha(\rho) = i\frac{g_{\sigma_f N} g_{\pi_1 N} g_{\pi_2 N}}{4m_N^2 E_{\pi_1} E_{\pi_2}}(k_{\pi_1}\cdot k_{\pi_2})\rho_{p(n)}, \tag{22}$$

$$i\Gamma_\beta = 0, \tag{23}$$

respectively. The calculational details of these are presented in Appendix B. We use the nucleon mass in the free space in Eq. (22). Its modification in the nuclear medium is small by including the one-loop diagram given in Fig. 4 which gives the leading contribution from the nuclear medium. The details of the calculation of the diagram are given in Appendix C.

4. Matrix element of $\eta \to 3\pi$ decay and numerical results

4.1. Matrix element of $\eta \to 3\pi$ decay

The tree-level diagrams that contribute to the $\eta \to 3\pi$ decay in the free space are shown in Fig. 5. We divide the contributions into three parts: the first part, $\mathcal{M}^{\pi^+\pi^-\pi^0}_{\rm contact}$, represented by diagrams (a) and (b), is the contributions from the 4-pseudoscalar meson contact vertices. The second one, $\mathcal{M}^{\pi^+\pi^-\pi^0}_{\rm isoscalar}$, given by diagrams (c), (d), (e), and (i), has the isoscalar mesons σ and f_0 in the intermediate state. The last one, $\mathcal{M}^{\pi^+\pi^-\pi^0}_{\rm isovector}$, obtained from diagrams (f), (g), (h), and (i), contains the isovector meson a_0. We shall see that $\mathcal{M}^{\pi^+\pi^-\pi^0}_{\rm isoscalar}$ gives the most significant contribution to the in-medium $\eta \to 3\pi$ decay width, which will be discussed in the next section. Diagrams (a), (b), (d), and (h) are the contributions from the $\eta - \pi_3$ and $\eta' - \pi_3$ mixing by ISB. The $\sigma - \sigma_3$ and $f_0 - \sigma_3$ mixings from ISB provide the contribution shown in diagram (i) in Fig. 5.

The matrix element of the $\eta \to \pi^+\pi^-\pi^0$ decay in the free space is written as follows:

$$\mathcal{M}^{\rm tree}_{\eta\to\pi^+\pi^-\pi^0} = \mathcal{M}^{\pi^+\pi^-\pi^0}_{\rm contact} + \mathcal{M}^{\pi^+\pi^-\pi^0}_{\rm isoscalar} + \mathcal{M}^{\pi^+\pi^-\pi^0}_{\rm isovector}, \tag{24}$$

$$\mathcal{M}^{\pi^+\pi^-\pi^0}_{\rm contact} = 2(-\sin\theta_{\pi^0\eta})g_{\pi_3\pi_3\pi^+\pi^-} + (-\sin\theta_{\pi^0\eta'}\frac{\sin 2\theta_{ps}}{2} + 2\sin\theta_{\pi^0\eta}\sin^2\theta_{ps})g_{\eta_0\eta_0\pi^+\pi^-}$$

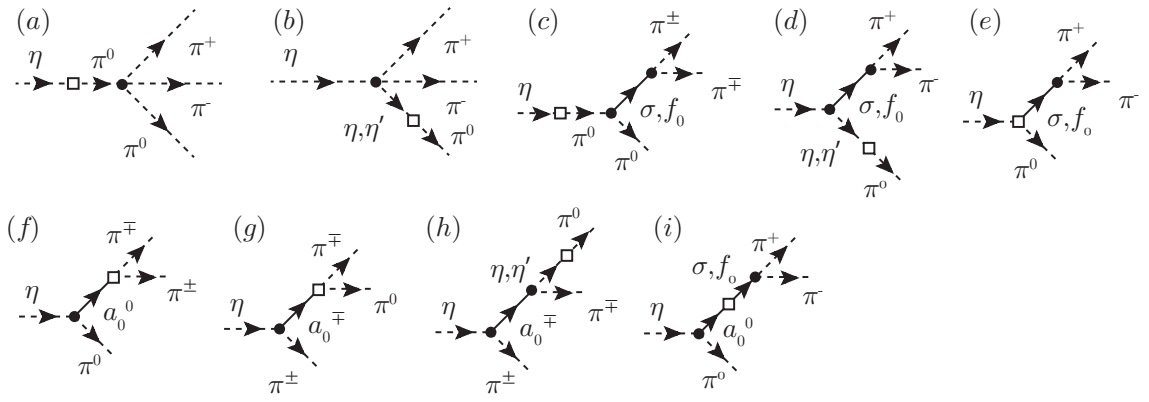

Fig. 5 The tree-level diagrams contributing to the $\eta \to 3\pi$ decay in the free space. The meanings of the lines are the same as those in Fig. 3. The vertex with the white box represents the effect of the isospin-symmetry breaking.

$$
\begin{aligned}
&+ (\sin\theta_{\pi^0\eta'}\cos^2\theta_{ps} - 2\sin\theta_{\pi^0\eta}\sin 2\theta_{ps}) g_{\eta_0\eta_8\pi^+\pi^-} \\
&+ (\sin\theta_{\pi^0\eta}\frac{\sin 2\theta_{ps}}{2} - 2\sin\theta_{\pi^0\eta}\cos^2\theta_{ps}) g_{\eta_0\eta_0\pi^+\pi^-}, \qquad (25)
\end{aligned}
$$

$$
\begin{aligned}
\mathcal{M}^{\pi^+\pi^-\pi^0}_{\rm isoscalar} = &-\Bigg\{ g_{\sigma\eta\pi^0}\frac{1}{s-m_\sigma^2}g_{\sigma\pi^+\pi^-} + g_{\eta\pi^0 f_0}\frac{1}{s-m_{f_0}^2}g_{f_0\pi^+\pi^-} \\
&+ 2(-\sin\theta_{\pi^0\eta})g_{\sigma\pi_3\pi_3}\frac{1}{s-m_\sigma^2}g_{\sigma\pi^+\pi^-} + 2(-\sin\theta_{\pi^0\eta})g_{\pi_3\pi_3 f_0}\frac{1}{s-m_{f_0}^2}g_{f_0\pi^+\pi^-} \\
&+ 2g_{\sigma\eta\eta}(\sin\theta_{\pi^0\eta})\frac{1}{s-m_\sigma^2}g_{\sigma\pi^+\pi^-} + 2g_{f_0\eta\eta}(\sin\theta_{\pi^0\eta})\frac{1}{s-m_{f_0}^2}g_{f_0\pi^+\pi^-} \\
&+ g_{\eta\eta'\sigma}(\sin\theta_{\pi^0\eta'})\frac{1}{s-m_\sigma^2}g_{\sigma\pi^+\pi^-} + g_{\eta\eta' f_0}(\sin\theta_{\pi^0\eta'})\frac{1}{s-m_{f_0}^2}g_{f_0\pi^+\pi^-} \\
&+ g_{a_0\pi^0\eta}\frac{1}{s-m_\sigma^2}g_{\sigma\pi^+\pi^-}(-\sin\theta_{\sigma_3\sigma}) + \frac{1}{s-m_{f_0}^2}g_{f_0\pi^+\pi^-}(-\sin\theta_{\sigma_3 f_0})\Bigg\}, \qquad (26)
\end{aligned}
$$

$$
\begin{aligned}
\mathcal{M}^{\pi^+\pi^-\pi^0}_{\rm isovector} = &-\Bigg\{ g_{\eta\pi^- a_0^+}\frac{1}{t-m_{a_0^-}^2}g_{a_0^-\pi^+\pi^0} + g_{\eta\pi^+ a_0^-}\frac{1}{u-m_{a_0^+}^2}g_{a_0^+\pi^-\pi^0} + g_{\eta\pi^0 a_0^0}\frac{1}{s-m_{a_0^0}^2}g_{a_0^0\pi^+\pi^-} \\
&+ g_{a_0^0\pi^0\eta}\frac{1}{s-m_{a_0^0}^2}g_{\sigma\pi^+\pi^-}(\sin\theta_{\sigma_3\sigma}) + g_{a_0^2\pi^0\eta}\frac{1}{s-m_{a_0^0}^2}g_{f_0\pi^+\pi^-}(\sin\theta_{\sigma_3 f_0}) \\
&+ g_{\eta\pi^- a_0^+}\frac{1}{t-m_{a_0^-}^2}g_{\eta\pi^+ a_0^-}(\sin\theta_{\pi^0\eta}) + g_{\eta\pi^+ a_0^-}\frac{1}{u-m_{a_0^+}^2}g_{\eta\pi^- a_0^+}(\sin\theta_{\pi^0\eta}) \\
&+ g_{\eta\pi^- a_0^+}\frac{1}{t-m_{a_0^-}^2}g_{\eta'\pi^+ a_0^-}(\sin\theta_{\pi^0\eta'}) + g_{\eta\pi^+ a_0^-}\frac{1}{u-m_{a_0^+}^2}g_{\eta'\pi^- a_0^+}(\sin\theta_{\pi^0\eta'})\Bigg\}. \qquad (27)
\end{aligned}
$$

The Mandelstam variables s, t, and u are defined as $s = (p_\eta - p_{\pi^0})^2$, $t = (p_\eta - p_{\pi^+})$, and $u = (p_\eta - p_{\pi^-})$, respectively. The couplings of mesons in the matrix elements are presented in Appendix B.1.

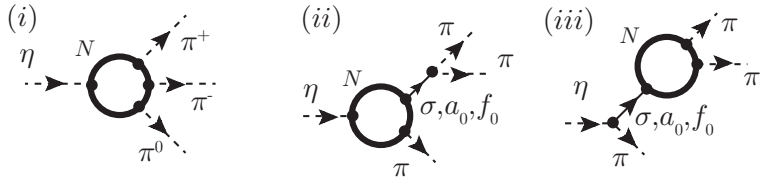

Fig. 6 Diagrams contributing to the $\eta \to 3\pi$ decay in the nuclear medium. The meanings of the lines are identical to those in Fig. 3.

The one-loop diagrams for the $\eta \to \pi^+\pi^-\pi^0$ decay in the nuclear medium are shown in Fig. 6. Diagram (i) in Fig. 6 leads to the in-medium correction of the 4-pseudoscalar meson coupling, while diagrams (ii) and (iii) in Fig. 6 lead to that of the scalar–2-pseudoscalar meson coupling. The resultant modification of the $\eta \to \pi^+\pi^-\pi^0$ decay amplitude $\delta\mathcal{M}^{\rm loop}_{\eta\to\pi^+\pi^-\pi^0}$ is given as follows:

$$\delta\mathcal{M}^{\rm loop}_{\eta\to\pi^+\pi^-\pi^0} = \delta\mathcal{M}^{\pi^+\pi^-\pi^0}_{\rm mixing} + \delta\mathcal{M}^{\pi^+\pi^-\pi^0}_{\rm isoscalar} + \delta\mathcal{M}^{\pi^+\pi^-\pi^0}_{\rm isovector}(\rho), \tag{28}$$

$$\delta\mathcal{M}^{\pi^+\pi^-\pi^0}_{\rm mixing} = +2(-\sin\theta_{\pi^0\eta})\Gamma_{\pi_3\pi_3\pi^+\pi^-} + 2(\sin\theta_{\pi^0\eta})\Gamma_{\eta\eta\pi^+\pi^-} + (\sin\theta_{\pi^0\eta'})\Gamma_{\eta\eta'\pi^+\pi^-}, \tag{29}$$

$$\begin{aligned}
\delta\mathcal{M}^{\pi^+\pi^-\pi^0}_{\rm isoscalar} =& -\frac{\Gamma_{\sigma\eta\pi_3}g^0_{\sigma\pi^+\pi^-}}{s-m_\sigma^2} - \frac{g^0_{\sigma\eta\pi_3}\Gamma_{\sigma\pi^+\pi^-}}{s-m_\sigma^2} - \frac{\Gamma_{f_0\eta\pi_3}g^0_{f_0\pi^+\pi^-}}{s-m_{f_0}^2} - \frac{g^0_{f_0\eta\pi_3}\Gamma_{f_0\pi^+\pi^-}}{s-m_{f_0}^2} \\
& - 2(-\sin\theta_{\pi^0\eta})\left\{\frac{\Gamma_{\sigma\pi_3\pi_3}g^0_{\sigma\sigma\pi^+\pi^-}}{s-m_\sigma^2} + \frac{g^0_{\sigma\pi_3\pi_3}\Gamma_{\sigma\sigma\pi^+\pi^-}}{s-m_\sigma^2} + \frac{\Gamma_{f_0\pi_3\pi_3}g^0_{f_0\sigma\pi^+\pi^-}}{s-m_{f_0}^2} + \frac{g^0_{f_0\pi_3\pi_3}\Gamma_{f_0\sigma\pi^+\pi^-}}{s-m_{f_0}^2}\right\} \\
& - 2(\sin\theta_{\pi^0\eta})\left\{\frac{\Gamma_{\sigma\eta\eta}g^0_{\sigma\pi^+\pi^-}}{s-m_\sigma^2} + \frac{g^0_{\sigma\eta\eta}\Gamma_{\sigma\pi^+\pi^-}}{s-m_\sigma^2} + \frac{\Gamma_{f_0\eta\eta}g^0_{f_0\pi^+\pi^-}}{s-m_{f_0}^2} + \frac{g^0_{f_0\eta\eta}\Gamma_{f_0\pi^+\pi^-}}{s-m_{f_0}^2}\right\} \\
& - (\sin\theta_{\pi^0\eta'})\left\{\frac{\Gamma_{\sigma\eta\eta'}g^0_{\sigma\pi^+\pi^-}}{s-m_\sigma^2} + \frac{g^0_{\sigma\eta\eta'}\Gamma_{\sigma\pi^+\pi^-}}{s-m_\sigma^2} + \frac{\Gamma_{f_0\eta\eta'}g^0_{f_0\pi^+\pi^-}}{s-m_{f_0}^2} + \frac{g^0_{f_0\eta\eta'}\Gamma_{f_0\pi^+\pi^-}}{s-m_{f_0}^2}\right\} \\
& - (\sin\theta_{\sigma_3\sigma})\left\{\frac{\Gamma_{a_0^0\eta\pi_3}g^0_{\sigma\pi^+\pi^-}}{s-m_\sigma^2} + \frac{g^0_{a_0^0\eta\pi_3}\Gamma_{\sigma\pi^+\pi^-}}{s-m_\sigma^2}\right\} - (\sin\theta_{\sigma_3 f_0})\left\{\frac{\Gamma_{a_0^0\eta\pi_3}g^0_{f_0\pi^+\pi^-}}{s-m_{f_0}^2} + \frac{g^0_{a_0^0\eta\pi_3}\Gamma_{f_0\pi^+\pi^-}}{s-m_{f_0}^2}\right\},
\end{aligned} \tag{30}$$

$$\begin{aligned}
\delta\mathcal{M}^{\pi^+\pi^-\pi^0}_{\rm isovector} =& -\frac{\Gamma_{a_0^+\eta\pi^-}g^0_{a_0^-\pi_3\pi^+}}{t-m^2_{a_0^\pm}} - \frac{\Gamma_{a_0^-\eta\pi^+}g^0_{a_0^+\pi_3\pi^-}}{u-m^2_{a_0^\pm}} - \frac{\Gamma_{a_0^0\eta\pi_3}g^0_{a_0^0\pi^+\pi^-}}{s-m^2_{a_0^0}} \\
& - (-\sin\theta_{\sigma_3\sigma})\left\{\frac{\Gamma_{a_0^0\eta\pi_3}g^0_{\sigma\pi^+\pi^-}}{s-m^2_{a_0^0}} + \frac{g^0_{a_0^0\eta\pi_3}\Gamma_{\sigma\pi^+\pi^-}}{s-m^2_{a_0^0}}\right\} - (-\sin\theta_{\sigma_3 f_0})\left\{\frac{\Gamma_{a_0^0\eta\pi_3}g^0_{f_0\pi^+\pi^-}}{s-m^2_{a_0^0}} + \frac{g^0_{a_0^0\eta\pi_3}\Gamma_{f_0\pi^+\pi^-}}{s-m^2_{a_0^0}}\right\} \\
& - (\sin\theta_{\pi^0\eta})\left\{\frac{\Gamma_{a_0^+\eta\pi^-}g^0_{a_0^-\eta\pi^+}}{t-m^2_{a_0^-}} + \frac{g^0_{a_0^+\eta\pi^-}\Gamma_{a_0^-\eta\pi^+}}{t-m^2_{a_0^-}} + \frac{\Gamma_{a_0^-\eta\pi^+}g^0_{a_0^+\eta\pi^-}}{u-m^2_{a_0^-}} + \frac{g^0_{a_0^-\eta\pi^+}\Gamma_{a_0^+\eta\pi^-}}{u-m^2_{a_0^-}}\right\} \\
& - (\sin\theta_{\pi^0\eta'})\left\{\frac{\Gamma_{a_0^+\eta\pi^-}g^0_{a_0^-\eta'\pi^+}}{t-m^2_{a_0^-}} + \frac{g^0_{a_0^+\eta\pi^-}\Gamma_{a_0^-\eta'\pi^+}}{t-m^2_{a_0^-}} + \frac{\Gamma_{a_0^-\eta\pi^+}g^0_{a_0^+\eta'\pi^-}}{u-m^2_{a_0^-}} + \frac{g^0_{a_0^-\eta\pi^+}\Gamma_{a_0^+\eta'\pi^-}}{u-m^2_{a_0^-}}\right\}.
\end{aligned} \tag{31}$$

The vertices with the superscript 0 are the couplings of the mesons in the free space. The one-loop vertex correction in the nuclear medium $\Gamma_{\sigma_f\pi_i\pi_j}$ is given in Eq. (22). The couplings of mesons and meson–nucleon are shown in Appendices B.1 and B.2. Here, the scalar meson

masses and the mixing angles are the in-medium values. The contribution from $\delta\mathcal{M}^{\pi^+\pi^-\pi^0}_{\rm mixing}$ in Eq. (29) does not exist because the correction of the 4-pseudoscalar meson vertex Γ_β vanishes as mentioned before. The matrix element in the nuclear medium is given as $\mathcal{M}_{\eta\to\pi^+\pi^-\pi^0}(\rho) = \mathcal{M}^{\rm tree}_{\eta\to\pi^+\pi^-\pi^0} + \delta\mathcal{M}^{\rm loop}_{\eta\to\pi^+\pi^-\pi^0}$.

Denoting the matrix element of the $\eta\to\pi^+\pi^-\pi^0$ process by $\mathcal{M}_{\eta\to\pi^+\pi^-\pi^0}(s,t,u)$, the decay amplitude of the $\eta\to 3\pi^0$ decay $\mathcal{M}_{\eta\to 3\pi^0}(s,t,u)$ is expressed as

$$\mathcal{M}_{\eta\to 3\pi^0}(s,t,u) = \mathcal{M}_{\eta\to\pi^+\pi^-\pi^0}(s,t,u) + \mathcal{M}_{\eta\to\pi^+\pi^-\pi^0}(t,u,s) + \mathcal{M}_{\eta\to\pi^+\pi^-\pi^0}(u,s,t), \quad (32)$$

owing to the Bose symmetry of the mesons [23]; note that our calculation only includes the leading-order effects of ISB.

4.2. Numerical results

The decay width Γ of the η meson to three pions is evaluated with the integration over the three-body phase space as

$$\Gamma = \frac{1}{(2\pi)^3}\frac{1}{32m_\eta^3}\frac{1}{n!}\int ds\int dt\,|\mathcal{M}|^2\,, \quad (33)$$

where n is the number of identical particles, and the phase space is evaluated using the meson masses in the free space. In the present study, the mass of the sigma meson in the free space $m_\sigma(\rho=0)$ is treated as a varying input as mentioned in Sect. 2: We show the results of the calculations using $m_\sigma(\rho=0) = 441, 550$, and 668 MeV as typical values in the following. The widths of the sigma meson in the free space for the respective sigma masses are evaluated as 124, 296, and 605 MeV.

The $\eta\to 3\pi$ decay width in the free space is fairly well reproduced in our model; the $\eta\to\pi^+\pi^-\pi^0$ and $3\pi^0$ decay widths in the free space are obtained as about 200 and 290 eV, which are about 70% of the respective experimental values [30]. The discrepancy may be attributed to the insufficient treatment of FSI, as mentioned in Sect. 1.

Here, we should remark on the valid range of the density of our calculation. Our calculation only takes account of the leading-order contribution of k_f, so the validity is limited in the small baryon density, as mentioned in Sect. 3. It is also problematic that the mass of the sigma meson becomes less than $2m_\pi$ at $\rho = 0.11$, 0.14, and 0.16 fm^{-3} for $m_\sigma(\rho=0) = 441$, 550, and 668 MeV, respectively, which could show that the tree-level approximation of the sigma meson is inadequate due to its small mass. Therefore, the valid density region of our calculation would be lower than the density although it may depend on the mass of the sigma meson in the free space.

In Fig. 7, we show the plot of the density dependence of the decay widths $\Gamma_{\eta\to\pi^+\pi^-\pi^0}(\rho)$ and $\Gamma_{\eta\to 3\pi^0}(\rho)$ in the symmetric nuclear medium up to ρ_0 with varying $m_\sigma(\rho=0)$. In the figures, dotted lines are used when the mass of the sigma meson becomes less than $2m_\pi$. From the figure, one can see an enhancement of the decay width with increasing baryon density ρ. We mention that both of the decay widths of $\eta\to\pi^+\pi^-\pi^0$ and $3\pi^0$ show a peak structure in Fig. 7. Here, we write ρ_c as the density at which the decay width is most enhanced for each $m_\sigma(\rho=0)$. ρ_c is given as 0.1, 0.13, and 0.15 fm^{-3} for $m_\sigma(\rho=0)$ =441, 550, and 668 MeV, respectively. The amount of the enhancement at $\rho=\rho_c$ depends on $m_\sigma(\rho=0)$; it becomes at most about four to ten times larger than the value in the free space. This originates from the stronger coupling of the sigma meson with the two-pion state for the larger $m_\sigma(\rho=0)$. On

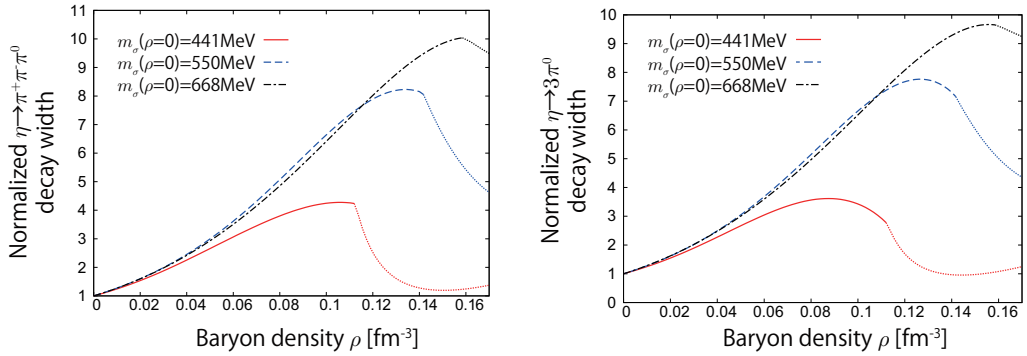

Fig. 7 Plots of the decay widths of $\eta \to \pi^+\pi^-\pi^0$ (left) and $\eta \to 3\pi^0$ (right) in the symmetric nuclear medium. The red solid, blue dashed, and black dashed-dotted lines are the plot of the decay widths with $m_\sigma(\rho = 0)$ =441, 550, and 668 MeV. A dotted line is used when the mass of the sigma meson is less than $2m_\pi$ for all inputs of $m_\sigma(\rho = 0)$. The decay widths of the $\eta \to \pi^+\pi^-\pi^0$ process at $\rho = 0$ are 192, 182, and 220 eV with $m_\sigma(\rho = 0)$ =441, 550, and 668 MeV. Those of $\eta \to 3\pi^0$ are 279, 265, and 317 eV.

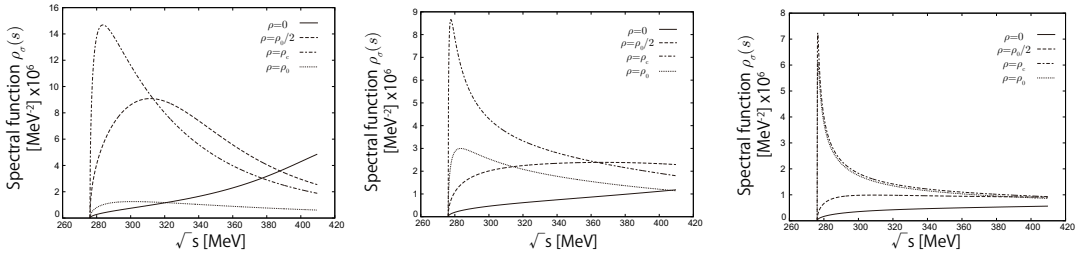

Fig. 8 The spectral functions of the sigma meson $\rho_\sigma(s)$ with the mass of the sigma meson in the free space 441 MeV (left), 550 MeV (center), and 668 MeV (right) varying the baryon number density ρ. The horizontal axis is $\sqrt{s}$ and the vertical axis is the spectral function times 10^6. The plot of the spectral function against $\sqrt{s}$ is limited in the range between $\sqrt{s_{\rm max}} = m_\eta - m_{\pi^0}$ and $\sqrt{s_{\rm min}} = 2m_{\pi^\pm}$. The spectral functions at $\rho = 0$, $\rho_0/2$, ρ_c, and ρ_0 are plotted in each figure. Here, $\rho_c = 0.1$, 0.13, and 0.15 fm^{-3} for $m_\sigma(\rho = 0) = 441$, 550, and 668 MeV where the $\eta \to 3\pi$ decay width is most enhanced for each $m_\sigma(\rho = 0)$.

the other hand, the dependence on $m_\sigma(\rho = 0)$ is relatively small at densities lower than $\rho_0/2$. The appearance of the peak at $\rho = \rho_c$ in Fig. 7 is associated with the approach of the sigma mass to the 2π threshold. To see this, we show the spectral function of the sigma meson $\rho_\sigma(s) = -{\rm Im}G_\sigma(s)/\pi$ in Fig. 8, where $G_\sigma(s)$ is the Green function of the sigma meson given in Eq. (20). One can see a growth of the peak near the 2π threshold accompanied by the increase of the baryon density in Fig. 8. The enhancement of the spectral function is most significant at $\rho = \rho_c$. Thus, the contributions from the sigma meson propagation in Eqs. (26) and (30) are enhanced in the nuclear medium. The locations of the cusps appearing in Fig. 7 correspond to the densities at which the mass of the sigma meson becomes as small as $2m_\pi$.

Next, we show the density dependence of the ratio of $\Gamma_{\eta\to3\pi^0}(\rho)$ to $\Gamma_{\eta\to\pi^+\pi^-\pi^0}(\rho)$ in Fig. 9. The plot shows a decrease of the ratio around ρ_c compared with the value at $\rho = 0$; i.e. the enhancement of the $\eta \to 3\pi^0$ decay width is weaker than that of the $\eta \to \pi^+\pi^-\pi^0$ decay

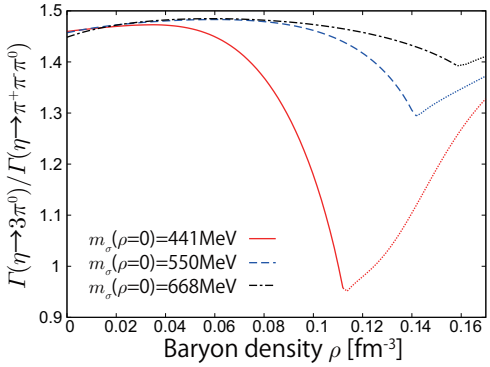

Fig. 9 The density dependence of the ratio of the decay width of $\eta \to 3\pi^0$ to that of $\eta \to \pi^+\pi^-\pi^0$ in the nuclear medium. The lines have the same meanings as those in Fig. 7.

around $\rho = \rho_c$. In the $\eta \to 3\pi^0$ decay, we simply write the contribution from the sigma meson to $\eta \to 3\pi^0$ $\mathcal{M}^{3\pi^0}_{\rm sigma}$ as

$$\mathcal{M}^{3\pi^0}_{\rm sigma} = -\frac{g_{\sigma\eta\pi}g_{\sigma\pi\pi}}{s-m_\sigma^2} - \frac{g_{\sigma\eta\pi}g_{\sigma\pi\pi}}{t-m_\sigma^2} - \frac{g_{\sigma\eta\pi}g_{\sigma\pi\pi}}{u-m_\sigma^2}. \tag{34}$$

When the Mandelstam variable s is near the 2π threshold, $s \sim 4m_\pi^2 \equiv s_{\rm min}$ and $t, u \sim (m_\eta^2 - m_\pi^2)/2 \equiv t_{\rm max}$. When the mass of the sigma meson is reduced within the range between $s_{\rm min}$ and $t_{\rm max}$ as the result of the softening of the sigma meson in the nuclear medium, the second and third terms of Eq. (34) have opposite signs to the first term. Thus, the degree of the enhancement of the $\eta \to 3\pi^0$ decay width is small compared with the $\eta \to \pi^+\pi^-\pi^0$ decay when the mass of the sigma meson decreases in the nuclear medium. This suppression becomes more severe in the case of the smaller $m_\sigma(\rho = 0)$ because the sigma-pole contribution plays a major role.

We comment on the uncertainty of the above results due to that of the decay width of the sigma meson; it can be modified from the tree-level value by quantum effects as we mentioned in Sect. 3. In Fig. 10, we show the plots of the decay widths of $\eta \to \pi^+\pi^-\pi^0$ and $3\pi^0$ in the nuclear medium taking account of the 30% modification of the width of the sigma meson from the tree-level value; Fig. 10 is plotted using $\Theta_{\rm tree}(p^2) \times 0.7$ and $\times 1.3$ as the decay width of the sigma meson where $\Theta_{\rm tree}(p^2)$ is the decay width at the tree level given in Eq. (21). As one can see from these figures, the difference is large in the high-density region. The difference from the tree-level value is about 40% at most, which is significant with the large mass of the sigma meson in the free space.

5. Conclusions and concluding remarks

In the present work, we have investigated the decay widths of the $\eta \to \pi^+\pi^-\pi^0$ and $3\pi^0$ processes in the nuclear medium using the linear sigma model focusing on the role of the softening of the sigma meson; the softening of the sigma meson in the nuclear medium is naturally taken into account in the model.

In the free space, our model gives a fairly good agreement with the experimental value; the obtained decay width is about 70% of the observed one [30]. The deficiency of our result in the free space may be attributed to an incomplete treatment of FSI, such as neglect of the ρ meson contribution.

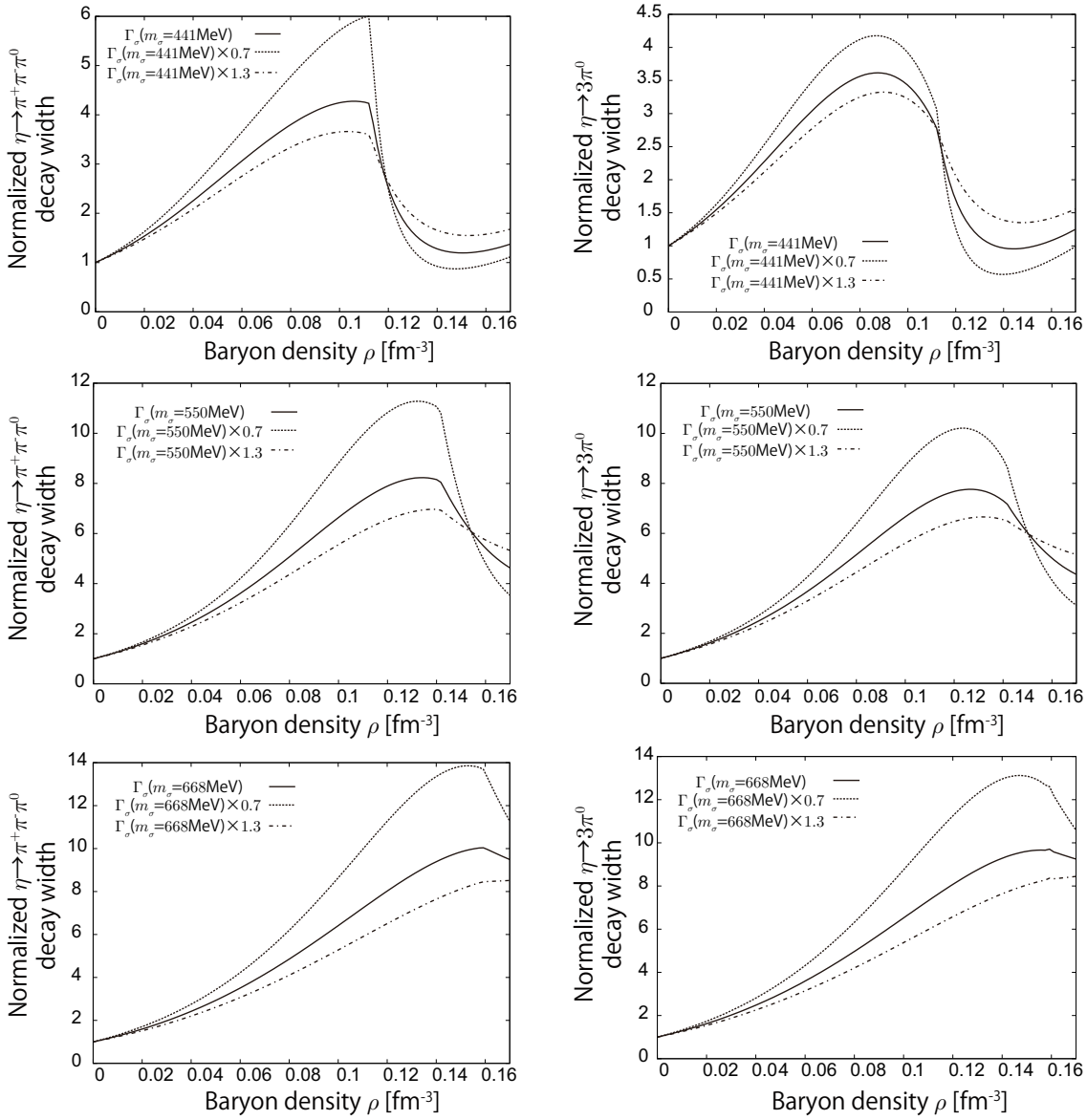

Fig. 10 Plot of the decay widths of the $\eta \to \pi^+\pi^-\pi^0$ (left panels) and $3\pi^0$ (right panels) processes by including the 30% uncertainty of the decay width of the sigma meson. The upper, middle, and lower panels for each column are plots of the decay width using $m_\sigma(\rho = 0) = 441, 550$, and 668 MeV, respectively. The $\eta \to 3\pi$ decay width evaluated using the tree-level decay width of the sigma meson is plotted with a solid line and that evaluated using the width of the sigma meson multiplied by a factor 0.7 (1.3) is plotted with a dotted (dash-dotted) line. The decay widths of $\eta \to \pi^+\pi^-\pi^0$ at $\rho = 0$ evaluated with the decay width of the sigma meson multiplied by 0.7 (1.3) are 197 (185), 178 (184), and 199 (235) eV for $m_\sigma(\rho = 0) = 441, 550$, and 668 MeV, respectively. Those of $\eta \to 3\pi^0$ are 286 (271), 260 (269), and 288 (340) eV.

For the calculation in the nuclear medium, the validity of our calculation is restricted within the small Fermi momentum k_f of the nuclear medium due to our limited calculations including only the leading-order contributions of k_f.

Our calculation shows that the enhancement becomes prominent when the sigma mass is near the 2π threshold. The decay widths become at most about four to ten times larger than the value at the free space, depending on the mass of the sigma meson in the free space which is a parameter of our model. The mechanism of the enhancement is attributed to the reduction of the mass of the sigma meson associated with the chiral restoration. It is worth emphasizing that the enhancement of the decay width is significant even at small density: For example, the decay width at $\rho = \rho_0/2$ is several times larger than that in the free space, and does not depend so much on the mass of the sigma meson in the free space. Thus, our claim is that the $\eta \to 3\pi$ decay in the nuclear medium could be a possible new probe for the chiral restoration.

It is worth mentioning here that the density dependence of the decay width of $\eta \to 3\pi^0$ is smaller than that of $\eta \to \pi^+\pi^-\pi^0$, owing to the Bose symmetry of the identical $3\pi^0$ in the final state and the softening of the sigma meson in the nuclear medium. The difference between the density dependences of the two decay widths should have significant importance in the possible experimental confirmation of the findings of the present study because the experimental determination of the ratio of the two final states seems much easier than that of the respective widths, which are small.

There is considerable room for elaboration of the present calculation. The contribution from the ρ meson can modify the density dependence of the decay width of the η meson. However, the modification is expected to be small at low density on which the present work is focused, although it can be significant at high density. We should undertake a more complete treatment of FSI and the nuclear medium. In particular, inclusion of the higher-order contribution of k_f is needed for a realistic argument; this contains the effect of the Fermi sea, which is necessary to determine the ground state in the nuclear medium properly. These are, however, beyond the scope of the present work, and are left for future projects.

Acknowledgments

We are grateful to K. Imai and H. Fujioka for informative discussions on the issues of a possible experimental confirmation of the present study. S.S. is a JSPS fellow and appreciates the support of a JSPS Grant-in-Aid (No. 25-1879). The work by T.K. is partially supported by a Grant-in-Aid for Scientific Research from JSPS (No. 24340054).

A. Calculation of meson self-energy in the nuclear medium

In this appendix, we perform the calculation of the meson self-energies in the nuclear medium and show the meson masses appearing in our calculations. The diagrams contributing to the meson masses are shown in Fig. 2.

First, we evaluate diagram (a) in Fig. 2. The contribution to the scalar meson self-energy is evaluated as follows;

$$-i\Sigma^{(a)} = -\frac{ig_{\sigma_f\sigma_1\sigma_2}g_{\sigma_f N}}{-m_{\sigma_f}^2}\mathrm{tr}\int\frac{d^4p}{(2\pi)^4}(-2\pi)(\not{p}+m_N)\delta(p^2-m_N^2)\theta(p_0)\theta(k_f-|\vec{p}|)$$

$$\sim -i\frac{g_{\sigma_f\sigma_1\sigma_2}g_{\sigma_f N}}{m_{\sigma_f}^2}\frac{4m_N}{(2\pi)^3}\frac{1}{2m_N}\frac{4\pi}{3}k_f^{p(n)3} = -i\frac{g_{\sigma_f\sigma_1\sigma_2}g_{\sigma_f N}}{m_{\sigma_f}^2}\rho_{p(n)}. \tag{A1}$$

Here, $k_f^{p(n)}$ is the Fermi momentum of the proton (neutron). From the first to the second line, we have made an approximation $E_N(\vec{p}) \sim m_N$, assuming that the nucleon mass is large enough. The pseudoscalar meson self-energy from diagram (a) in Fig. 2 is calculated in much the same way as the case of the scalar meson one, other than the coupling $g_{\sigma_f\sigma_1\sigma_2}$ and $g_{\sigma_f\pi_1\pi_2}$.

Next, we evaluate the contributions from diagrams (b) and (c) in Fig. 2 for the scalar and pseudoscalar mesons. Diagram (b) for the self-energy of the scalar meson is given as

$$\begin{aligned}
-i\Sigma_s^{(b)} =& -\mathrm{tr}\int\frac{d^4p}{(2\pi)^4}(-ig_{\sigma_1 N})\frac{i(\not{p}+\not{q}+m_N)}{(p+q)^2-m_N^2}(-ig_{\sigma_2 N})(-2\pi)(\not{p}+m_N)\delta(p^2-m_N^2)\theta(p_0)\theta(k_f-|\vec{p}|)\\
=& -ig_{\sigma_1 N}g_{\sigma_2 N}\int\frac{d^4p}{(2\pi)^3}\frac{4[p\cdot(p+q)+m_N^2]}{2p\cdot q+q^2}\frac{1}{2E_N(\vec{p})}\delta(p_0-E_N(\vec{p}))\theta(k_f-|\vec{p}|)\\
\sim& -4ig_{\sigma_1 N}g_{\sigma_2 N}\frac{2m_N^2+m_Nm_s}{2m_Nm_s+m_s^2}\frac{1}{2m_N}\frac{1}{(2\pi)^3}\frac{4\pi}{3}k_f^3 = -ig_{\sigma_1 N}g_{\sigma_2 N}\frac{\rho_{p(n)}}{m_{\sigma_1}}.
\end{aligned} \tag{A2}$$

From the second to the third line, $E_N(\vec{p})$ is approximated by m_N as before. In a similar manner, diagram (c) is evaluated as

$$\begin{aligned}
-i\Sigma_s^{(c)} =& -\mathrm{tr}\int\frac{d^4p}{(2\pi)^4}(-ig_{\sigma_2 N})\frac{i(\not{p}+m_N)}{p^2-m_N^2}(-ig_{\sigma_1 N})(-2\pi)(\not{p}+\not{q}+m_N)\delta((p+q)^2-m_N^2)\\
&\times\theta(p_0+q_0)\theta(k_f-|\vec{p}+\vec{q}|)\\
=& -ig_{\sigma_1 N}g_{\sigma_2 N}\mathrm{tr}\int\frac{d^4p}{(2\pi)^3}\frac{\not{p}-\not{q}+m_N}{(p-q)^2-m_N^2}\frac{\not{p}+m_N}{2E_N(\vec{p})}\delta(p_0-E_N(\vec{p}))\theta(k_f-|\vec{p}|)\\
=& -ig_{\sigma_1 N}g_{\sigma_2 N}\int\frac{d^4p}{(2\pi)^3}\frac{p\cdot(p-q)+m_N^2}{(p-q)^2-m_N^2}\frac{1}{2E_N(\vec{p})}\delta(p_0-E_N(\vec{p}))\theta(k_f-|\vec{p}|)\\
\sim& -4ig_{\sigma_1 N}g_{\sigma_2 N}\frac{2m_N^2-m_Nm_s}{-2m_Nm_s+m_s^2}\frac{1}{2m_N}\frac{1}{(2\pi)^3}\frac{4\pi}{3}k_f^{p(n)3} = ig_{\sigma_1 N}g_{\sigma_2 N}\frac{\rho_{p(n)}}{m_{\sigma_1}}
\end{aligned} \tag{A3}$$

From the first to the second line, we have changed the integration variable p to $p-q$.

As in the case of the above calculations, the self-energies of the pseudoscalar meson from diagrams (b) and (c) in Fig. 2 are evaluated as

$$\begin{aligned}
-i\Sigma_{ps}^{(b)} =& -\mathrm{tr}\int\frac{d^4p}{(2\pi)^4}(g_{\pi_1 N}\gamma_5)\frac{i(\not{p}+\not{q}+m_N)}{(p+q)^2-m_N^2}(g_{\pi_2 N}\gamma_5)(\not{p}+m_N)(-2\pi)\delta(p^2-m_N^2)\\
&\times\theta(p_0)\theta(k_f-|\vec{p}|)\\
=& ig_{\pi_1 N}g_{\pi_2 N}\int\frac{d^4p}{(2\pi)^3}\frac{4[-p\cdot(p+q)+m_N^2]}{(p+q)^2-m_N^2}\frac{1}{2E_N(\vec{p})}\delta(p_0-E_N(\vec{p}))\theta(k_f-|\vec{p}|)\\
\sim& ig_{\pi_1 N}g_{\pi_2 N}\frac{1}{(2\pi)^3}\frac{-4m_Nm_{ps}}{2m_Nm_{ps}+m_{ps}^2}\frac{1}{2m_N}\frac{4\pi}{3}k_f^{p(n)3} \sim -i\frac{g_{\pi_1 N}g_{\pi_2 N}}{2m_N}\rho_{p(n)}
\end{aligned} \tag{A4}$$

and

$$\begin{aligned}
-i\Sigma_{ps}^{(c)} =& -\mathrm{tr}\int\frac{d^4p}{(2\pi)^4}(g_{\pi_2 N}\gamma_5)\frac{i(\not{p}+m_N)}{p^2-m_N^2}(g_{\pi_1 N}\gamma_5)(-2\pi)(\not{p}+\not{q}+m_N)\delta((p+q)^2-m_N^2)\\
&\times\theta(p_0+q_0)\theta(k_f-|\vec{p}+\vec{q}|)
\end{aligned}$$

$$
\begin{aligned}
=&ig_{\pi_1 N}g_{\pi_2 N}\int\frac{d^4p}{(2\pi)^3}\frac{4[p\cdot(-p+q)+m_N^2]}{(p-q)^2-m_N^2}\frac{1}{2E_N(\vec{p})}\delta(p_0-E_N(\vec{p}))\theta(k_f-|\vec{p}|)\\
=&ig_{\pi_1 N}g_{\pi_2 N}\int\frac{d^4p}{(2\pi)^3}\int\frac{d^4p}{(2\pi)^3}\frac{4p\cdot q}{-2p\cdot q+q^2}\frac{1}{2E_N(\vec{p})}\theta(k_f-|\vec{p}|)\\
\sim&-ig_{\pi_1 N}g_{\pi_2 N}\frac{1}{(2\pi)^3}\frac{4m_N m_{ps}}{2m_N m_{ps}-m_{ps}^2}\frac{1}{2m_N}\frac{4\pi}{3}k_f^{p(n)3}\sim-i\frac{g_{\pi_1 N}g_{\pi_2 N}}{2m_N}\rho_{p(n)}. \qquad \text{(A5)}
\end{aligned}
$$

In the last lines of Eqs. (A4) and (A5), we have dropped m_{ps} regarding it as small compared with the nucleon mass m_N. Thus, the self-energies of mesons, $\Sigma_s(\rho)$ and $\Sigma_{ps}(\rho)$, are given as

$$
-i\Sigma_s(\rho)=-i\frac{g_{\sigma_k N}g_{\sigma_k\sigma_1\sigma_2}}{m_{\sigma_k}^2}\rho_{p(n)}, \qquad \text{(A6)}
$$

$$
-i\Sigma_{ps}(\rho)=-i\frac{g_{\sigma_k N}g_{\sigma_k\pi_1\pi_2}}{m_{\sigma_k}^2}\rho_{p(n)}-i\frac{g_{\pi_1 N}g_{\pi_2 N}}{m_N}\rho_{p(n)}. \qquad \text{(A7)}
$$

Thus, the meson masses in the nuclear medium are given as follows:

$$
\begin{aligned}
m_{\pi_3}^2(\rho)=&m_{\pi^\pm}^2(\rho)=m_{\pi^{\pm,0}}^2+2\lambda\langle\sigma_q\rangle\delta\langle\sigma_q\rangle+2\lambda'(2\langle\sigma_q\rangle\delta\langle\sigma_q\rangle+\langle\sigma_s\rangle\delta\langle\sigma_s\rangle)\\
&+\frac{2}{3}B(2\delta\langle\sigma_q\rangle+\delta\langle\sigma_s\rangle)+\frac{g^2\rho}{2m_N}, \qquad \text{(A8)}\\
m_{\eta_0}^2(\rho)=&m_{\eta_0}^2+\frac{2}{3}\lambda(\langle\sigma_q\rangle\delta\langle\sigma_q\rangle+2\langle\sigma_s\rangle\delta\langle\sigma_s\rangle)+2\lambda'(2\langle\sigma_q\rangle\delta\langle\sigma_q\rangle+\langle\sigma_s\rangle\delta\langle\sigma_s\rangle)\\
&+\frac{2}{3}B(2\delta\langle\sigma_q\rangle+\delta\langle\sigma_s\rangle)+\frac{g^2\rho}{3m_N}, \qquad \text{(A9)}\\
m_{\eta_8}^2(\rho)=&m_{\eta_8}^2+\frac{2}{3}\lambda(\langle\sigma_q\rangle\delta\langle\sigma_q\rangle+2\langle\sigma_s\rangle\delta\langle\sigma_s\rangle)+2\lambda'(2\langle\sigma_q\rangle\delta\langle\sigma_q\rangle+\langle\sigma_s\rangle\delta\langle\sigma_s\rangle)\\
&-\frac{B}{3}(4\delta\langle\sigma_q\rangle-\delta\langle\sigma_s\rangle)+\frac{g^2\rho}{6m_N}, \qquad \text{(A10)}\\
m_{\eta_0\eta_8}^2(\rho)=&m_{\eta_0\eta_8}^2+\frac{4\lambda}{3\sqrt{2}}(\langle\sigma_q\rangle\delta\langle\sigma_q\rangle-\langle\sigma_s\rangle\delta\langle\sigma_s\rangle)-\frac{\sqrt{2}}{3}B(\delta\langle\sigma_q\rangle-\delta\langle\sigma_s\rangle)+\frac{g^2\rho}{3\sqrt{2}m_N}, \qquad \text{(A11)}\\
m_{\eta_0\pi_3}^2(\rho)=&m_{\eta_0\pi_3}^2-2\sqrt{\frac{2}{3}}\delta\langle\delta\sigma_q\rangle(2\lambda\langle\sigma_q\rangle-B)-4\sqrt{\frac{2}{3}}\lambda\langle\delta\sigma_q\rangle\delta\langle\sigma_q\rangle-\frac{g^2\delta\rho}{\sqrt{6}m_N}, \qquad \text{(A12)}\\
m_{\pi_3\eta_8}^2(\rho)=&m_{\pi_3\eta_8}^2-\frac{4}{\sqrt{3}}\delta\langle\delta\sigma_q\rangle(\lambda\langle\sigma_q\rangle+B)-\frac{4}{\sqrt{3}}\lambda\langle\delta\sigma_q\rangle\delta\langle\sigma_q\rangle-\frac{g^2\delta\rho}{2\sqrt{3}m_N}. \qquad \text{(A13)}
\end{aligned}
$$

Due to ISB, the masses of the pseudoscalar mesons are modified as follows;

$$
\begin{aligned}
m_{\pi^0}^2=&m_{\pi_3}^2-\frac{(m_{\pi_3\eta'}^2)^2}{m_{\eta'}^{(is)2}-m_{\pi_3}^2}-\frac{(m_{\pi_3\eta}^2)^2}{m_{\eta}^{(is)2}-m_{\pi_3}^2}, \qquad \text{(A14)}\\
m_{\eta'}^2=&m_{\eta'}^{(is)2}+\frac{(m_{\pi_3\eta'}^2)^2}{m_{\eta'}^{(is)2}-m_{\pi_3}^2}, \qquad \text{(A15)}\\
m_{\eta}^2=&m_{\eta}^{(is)2}+\frac{(m_{\pi_3\eta}^2)^2}{m_{\eta}^{(is)2}-m_{\pi_3}^2}. \qquad \text{(A16)}
\end{aligned}
$$

The modifications of the meson masses through the mixing of π_3-η or π_3-η' are ignored in this calculation because they are $O((m_u-m_d)^2)$. Here, $m_{\eta,\eta'}^{(is)2}$ are the masses of the η,η' mesons

in the isospin-symmetric limit; $m^{(is)2}_{\eta',\eta} = (m^2_{\eta_0} + m^2_{\eta_8} \pm \sqrt{(m^2_{\eta_0} - m^2_{\eta_8})^2 + 4(m^2_{\eta_0\eta_8})^2})/2$. $m^2_{\pi_3\eta}$ and $m^2_{\pi_3\eta'}$ are given as $m^2_{\pi_3\eta} = -\sin\theta_{ps} m^2_{\pi_3\eta_0} + \cos\theta_{ps} m^2_{\pi_3\eta_8}$, $m^2_{\pi_3\eta'} = \cos\theta_{ps} m^2_{\pi_3\eta_0} + \sin\theta_{ps} m^2_{\pi_3\eta_8}$.

The mixing angles are defined as

$$\begin{aligned}\begin{pmatrix}\pi^0\\ \eta'\\ \eta\end{pmatrix} &= \begin{pmatrix}\cos\theta_{\pi_3\eta} & & \sin\theta_{\pi_3\eta}\\ & 1 & \\ -\sin\theta_{\pi_3\eta} & & \cos\theta_{\pi_3\eta}\end{pmatrix}\begin{pmatrix}\cos\theta_{\pi_3\eta'} & \sin\theta_{\pi_3\eta'} & \\ -\sin\theta_{\pi_3\eta'} & \cos\theta_{\pi_3\eta'} & \\ & & 1\end{pmatrix}\begin{pmatrix}1 & & \\ & \cos\theta_{ps} & \sin\theta_{ps}\\ & -\sin\theta_{ps} & \cos\theta_{ps}\end{pmatrix}\begin{pmatrix}\pi_3\\ \eta_0\\ \eta_8\end{pmatrix}\\ &\sim \begin{pmatrix}\pi_3 + \sin\theta_{\pi_3\eta'}\eta'^{(is)} + \sin\theta_{\pi_3\eta}\eta^{(is)}\\ \eta'^{(is)} - \sin\theta_{\pi_3\eta'}\pi_3\\ \eta^{(is)} - \sin\theta_{\pi_3\eta}\pi_3\end{pmatrix}. \end{aligned} \tag{A17}$$

From the first to the second line, we omit the $O((m_u - m_d)^2)$ terms. Here, we set $\eta'^{(is)} = \cos\theta_{ps}\eta_0 + \sin\theta_{ps}\eta_8$ and $\eta^{(is)} = -\sin\theta_{ps}\eta_0 + \cos\theta_{ps}\eta_8$. The mixing angles between η-π^0 and η'-π^0 are given as follows:

$$\tan 2\theta_{ps} = \frac{2m^2_{\eta_0\eta_8}}{m^2_{\eta_0} - m^2_{\eta_8}}, \tag{A18}$$

$$\tan 2\theta_{\pi^0\eta} = \frac{2m^2_{\pi_3\eta}}{m^2_{\pi_3} - m^{(is)2}_{\eta}}, \tag{A19}$$

$$\tan 2\theta_{\pi^0\eta'} = \frac{2m^2_{\pi_3\eta'}}{m^2_{\pi_3} - m^{(is)2}_{\eta'}}. \tag{A20}$$

In the same way as before, the mixing of scalar mesons can be written as follows;

$$\begin{aligned}\begin{pmatrix}a^0_0\\ \sigma\\ f_0\end{pmatrix} &= \begin{pmatrix}\cos\theta_{\sigma_3 f_0} & & \sin\theta_{\sigma_3 f_0}\\ & 1 & \\ -\sin\theta_{\sigma_3 f_0} & & \cos\theta_{\sigma_3 f_0}\end{pmatrix}\begin{pmatrix}\cos\theta_{\sigma_3\sigma} & \sin\theta_{\sigma_3\sigma} & \\ -\sin\theta_{\sigma_3\sigma} & \cos\theta_{\sigma_3\sigma} & \\ & & 1\end{pmatrix}\begin{pmatrix}1 & & \\ & \cos\theta_s & \sin\theta_s\\ & -\sin\theta_s & \cos\theta_s\end{pmatrix}\begin{pmatrix}\sigma_3\\ \sigma_0\\ \sigma_8\end{pmatrix}\\ &\sim \begin{pmatrix}\sigma_3 + \sin\theta_{\sigma_3\sigma}\sigma^{(is)} + \sin\theta_{\sigma_3 f_0} f^{(is)}_0\\ \sigma^{(is)} - \sin\theta_{\sigma_3\sigma}\sigma_3\\ f^{(is)}_0 - \sin\theta_{\sigma_3 f_0}\sigma_3\end{pmatrix} \end{aligned} \tag{A21}$$

The mixing angles are given as follows:

$$m^2_\sigma = m^{(is)2}_\sigma - \frac{(m^2_{\sigma_3\sigma})^2}{m^2_{\sigma_3} - m^{(is)2}_\sigma}, \tag{A22}$$

$$m^2_{f_0} = m^{(is)2}_{f_0} + \frac{(m^2_{\sigma_3 f_0})^2}{m^{(is)2}_{f_0} - m^{(is)2}_{\sigma_3}}, \tag{A23}$$

$$m^2_{a_0} = m^2_{\sigma_3} + \frac{(m^2_{\sigma_3\sigma})^2}{m^2_{\sigma_3} - m^{(is)2}_\sigma} - \frac{(m^2_{\sigma_3 f_0})^2}{m^{(is)2}_{f_0} - m^2_{\sigma_3}}, \tag{A24}$$

$$\tan 2\theta_s = \frac{2m^2_{\sigma_0\sigma_8}}{m^2_{\sigma_0} - m^2_{\sigma_8}}, \tag{A25}$$

$$\tan 2\theta_{\sigma_3\sigma} = \frac{2m^2_{\sigma_3\sigma}}{m^2_{\sigma_3} - m^{(is)2}_\sigma}, \tag{A26}$$

$$\tan 2\theta_{\sigma_3 f_0} = \frac{2m^2_{\sigma_3 f_0}}{m^2_{\sigma_3} - m^{(is)2}_{\sigma}}, \tag{A27}$$

where $m^2_{\sigma_3\sigma} = \cos\theta_s m^2_{\sigma_0\sigma_3} + \sin\theta_s m^2_{\sigma_3\sigma_8}$ and $m^2_{\sigma_3 f_0} = -\sin\theta_2 m^2_{\sigma_0\sigma_3} + \cos\theta_s m^2_{\sigma_3\sigma_8}$. The corrections of the scalar meson masses from the mixing are ignored in this calculation, as in the case of the pseudoscalar meson masses.

$m^2_{ij} = \partial^2 V_{\rm eff}/\partial\sigma_i\partial\sigma_j$ $(i,j = u,d,s)$ appearing in Sect. 2 are written as

$$m^2_{uu} = \mu^2 + 3\lambda\langle\sigma_u\rangle^2 + \lambda'(3\langle\sigma_u\rangle^2 + \langle\sigma_d\rangle^2 + \langle\sigma_s\rangle^2) \tag{A28}$$

$$m^2_{ud} = 2\lambda'\langle\sigma_u\rangle\langle\sigma_d\rangle - B\langle\sigma_s\rangle \tag{A29}$$

$$m^2_{us} = 2\lambda'\langle\sigma_u\rangle\langle\sigma_s\rangle - B\langle\sigma_d\rangle \tag{A30}$$

$$m^2_{dd} = \mu^2 + 3\lambda\langle\sigma_d\rangle^2 + \lambda'(\langle\sigma_u\rangle^2 + 3\langle\sigma_d\rangle^2 + \langle\sigma_s\rangle^2) \tag{A31}$$

$$m^2_{ds} = 2\lambda'\langle\sigma_d\rangle\langle\sigma_s\rangle - B\langle\sigma_u\rangle \tag{A32}$$

$$m^2_{ss} = \mu^2 + 3\lambda\langle\sigma_s\rangle^2 + \lambda'(\langle\sigma_u\rangle^2 + \langle\sigma_d\rangle^2 + 3\langle\sigma_s\rangle^2) \tag{A33}$$

B. Couplings of mesons

In this appendix, we present explicit forms of the tree-level couplings of mesons and meson–baryon appearing in the text and show the calculations of the in-medium corrections of the vertices. The modification of the vertices of mesons comes from the diagrams shown in Fig. 3. Here, the momenta of the outgoing meson π_i, incoming mesons σ_f, and the η meson in the initial state are denoted by k_i, $\tilde{q} = k_1 + k_2$, and $q = k_1 + k_2 + k_3$, respectively. We write the mass of the meson with the external momenta k_i as m_i. Furthermore, the coupling of the meson π_i and nucleon $g_{\pi_i N}$ is given by g_i for short. The tree-level couplings of mesons are shown in Appendices B.1. The meson–baryon couplings at tree level are given in Appendix B.2. Appendix B.3 and B.4 give the calculation of the in-medium modification of the scalar–2-pseudoscalar and the 4-pseudoscalar meson couplings, respectively.

B.1. Tree-level couplings of mesons

Here, we show the tree-level couplings of the mesons. The 4-pseudoscalar meson and the scalar–2-pseudoscalar meson couplings at tree level are obtained as the coefficients of the $\pi_i\pi_j\pi_k\pi_l$ and $\sigma_f\pi_i\pi_j$ terms in the Lagrangian of LσM given in Eq. (1). The tree-level 4-point couplings of pseudoscalar mesons $g_{\pi_i\pi_j\pi_k\pi_l}$ are given as

$$g_{\pi^+\pi^-\pi_3\pi_3} = -(\frac{\lambda}{2} + \lambda'), \tag{B1}$$

$$g_{\pi^+\pi^-\eta_0\eta_0} = -(\lambda + \lambda'), \tag{B2}$$

$$g_{\pi^+\pi^-\eta_0\eta_8} = -\sqrt{2}\lambda, \tag{B3}$$

$$g_{\pi^+\pi^-\eta_8\eta_8} = -\left(\frac{\lambda}{2} + \lambda'\right), \tag{B4}$$

and the scalar–2-pseudosclar couplings $g_{\sigma_i\pi_j\pi_k}$ are given as follows:

$$g_{\sigma_0\pi^+\pi^-} = -\left(\frac{\lambda}{\sqrt{3}}(\langle\sigma_u\rangle + \langle\sigma_d\rangle) + \frac{2\lambda'}{\sqrt{3}}(\langle\sigma_u\rangle + \langle\sigma_d\rangle + \langle\sigma_s\rangle) - \frac{B}{\sqrt{3}}\right), \tag{B5}$$

$$g_{\sigma_3\pi^+\pi^-} = -\left(\frac{3}{\sqrt{2}}\lambda + \sqrt{2}\lambda'\right)(\langle\sigma_u\rangle - \langle\sigma_d\rangle), \tag{B6}$$

$$g_{\sigma_8\pi^+\pi^-} = -\left(\frac{\lambda}{\sqrt{6}}(\langle\sigma_u\rangle + \langle\sigma_d\rangle) + \frac{2}{\sqrt{6}}\lambda'(\langle\sigma_u\rangle + \langle\sigma_d\rangle - 2\langle\sigma_s\rangle) + \frac{2}{\sqrt{6}}B\right), \tag{B7}$$

$$g_{\sigma_0\pi_3\pi_3} = -\left(\frac{\lambda}{2\sqrt{3}}(\langle\sigma_u\rangle + \langle\sigma_d\rangle) + \frac{\lambda'}{\sqrt{3}}(\langle\sigma_u\rangle + \langle\sigma_d\rangle + \langle\sigma_s\rangle) - \frac{B}{2\sqrt{3}}\right), \tag{B8}$$

$$g_{\sigma_8\pi_3\pi_3} = -\left(\frac{\lambda}{2\sqrt{6}}(\langle\sigma_u\rangle + \langle\sigma_d\rangle) + \frac{\lambda'}{\sqrt{6}}(\langle\sigma_u\rangle + \langle\sigma_d\rangle - 2\langle\sigma_s\rangle) + \frac{B}{\sqrt{6}}\right), \tag{B9}$$

$$g_{\sigma_0\eta_0\eta_0} = -\left(\frac{\lambda}{3\sqrt{3}}(\langle\sigma_u\rangle + \langle\sigma_d\rangle + \langle\sigma_s\rangle) + \frac{\lambda'}{\sqrt{3}}(\langle\sigma_u\rangle + \langle\sigma_d\rangle + \langle\sigma_s\rangle) + \frac{B}{\sqrt{3}}\right), \tag{B10}$$

$$g_{\sigma_8\eta_0\eta_0} = -\left(\frac{\lambda}{3\sqrt{6}}(\langle\sigma_u\rangle + \langle\sigma_d\rangle - 2\langle\sigma_s\rangle) + \frac{\lambda'}{\sqrt{6}}(\langle\sigma_u\rangle + \langle\sigma_d\rangle - 2\langle\sigma_s\rangle)\right), \tag{B11}$$

$$g_{\sigma_0\eta_8\eta_8} = -\left(\frac{\lambda}{6\sqrt{3}}(\langle\sigma_u\rangle + \langle\sigma_d\rangle + 4\langle\sigma_s\rangle) + \frac{\lambda'}{\sqrt{3}}(\langle\sigma_u\rangle + \langle\sigma_d\rangle + \langle\sigma_s\rangle) - \frac{B}{2\sqrt{3}}\right), \tag{B12}$$

$$g_{\sigma_8\eta_8\eta_8} = -\left(\frac{\lambda}{6\sqrt{6}}(\langle\sigma_u\rangle + \langle\sigma_d\rangle - 8\langle\sigma_s\rangle) + \frac{\lambda'}{\sqrt{6}}(\langle\sigma_u\rangle + \langle\sigma_d\rangle - 2\langle\sigma_s\rangle) - \frac{B}{\sqrt{6}}\right), \tag{B13}$$

$$g_{\sigma_0\eta_0\eta_8} = -\frac{2}{3\sqrt{6}}\lambda(\langle\sigma_u\rangle + \langle\sigma_d\rangle - 2\langle\sigma_s\rangle), \tag{B14}$$

$$g_{\sigma_8\eta_0\eta_8} = -\left(\frac{\lambda}{3\sqrt{3}}(\langle\sigma_u\rangle + \langle\sigma_d\rangle + 4\langle\sigma_s\rangle) - \frac{B}{\sqrt{3}}\right), \tag{B15}$$

$$g_{\sigma_0\pi_3\eta_0} = -\frac{\sqrt{2}}{3}\lambda(\langle\sigma_u\rangle - \langle\sigma_d\rangle), \tag{B16}$$

$$g_{\sigma_3\pi_3\eta_0} = -\left(\frac{\lambda}{\sqrt{3}}(\langle\sigma_u\rangle + \langle\sigma_d\rangle) - \frac{B}{\sqrt{3}}\right), \tag{B17}$$

$$g_{\sigma_8\pi_3\eta_0} = -\frac{\lambda}{3}(\langle\sigma_u\rangle - \langle\sigma_d\rangle), \tag{B18}$$

$$g_{\sigma_0\pi_3\eta_8} = -\frac{\lambda}{3}(\langle\sigma_u\rangle - \langle\sigma_d\rangle), \tag{B19}$$

$$g_{\sigma_3\pi_3\eta_8} = -\left(\frac{\lambda}{\sqrt{6}}(\langle\sigma_u\rangle + \langle\sigma_d\rangle) + \frac{2}{\sqrt{6}}B\right), \tag{B20}$$

$$g_{\sigma_8\pi_3\eta_8} = -\frac{\lambda}{3\sqrt{2}}(\langle\sigma_u\rangle - \langle\sigma_d\rangle), \tag{B21}$$

$$g_{a_0^\pm\eta_0\pi^\mp} = -\left(\frac{\lambda}{\sqrt{3}}(\langle\sigma_u\rangle + \langle\sigma_d\rangle) - \frac{B}{\sqrt{3}}\right), \tag{B22}$$

$$g_{a_0^\pm\pi_3\pi^\mp} = -\left(-\frac{\lambda}{\sqrt{2}}(\langle\sigma_u\rangle - \langle\sigma_d\rangle)\right), \tag{B23}$$

$$g_{a_0^\pm\eta_8\pi^\mp} = -\left(\frac{\lambda}{\sqrt{6}}(\langle\sigma_u\rangle + \langle\sigma_d\rangle) + \frac{2}{\sqrt{6}}B\right) \tag{B24}$$

Due to the mixing of the mesons, the couplings are modified as follows:

$$g_{\sigma\pi^0\pi^0} = \cos\theta_s g_{\sigma_0\pi_3\pi_3} + \sin\theta_s g_{\sigma_8\pi_3\pi_3}, \tag{B25}$$

$$g_{f_0\pi^0\pi^0} = -\sin\theta_s g_{\sigma_0\pi_3\pi_3} + \cos\theta_s g_{\sigma_8\pi_3\pi_3}, \tag{B26}$$

$$g_{\sigma\pi^+\pi^-} = \cos\theta_s g_{\sigma_0\pi^+\pi^-} + \sin\theta_s g_{\sigma_8\pi^+\pi^-}, \tag{B27}$$

$$g_{f_0\pi^+\pi^-} = -\sin\theta_s g_{\sigma_0\pi^+\pi^-} + \cos\theta_s g_{\sigma_8\pi^+\pi^-}, \tag{B28}$$

$$\begin{aligned} g_{\sigma\eta\eta} =& \cos\theta_s \left(\sin^2\theta_{ps} g_{\sigma_0\eta_0\eta_0} - \sin 2\theta_{ps} g_{\sigma_0\eta_0\eta_8} + \cos^2\theta_{ps} g_{\sigma_0\eta_8\eta_8}\right) \\ &+ \sin\theta_s \left(\sin^2\theta_{ps} g_{\sigma_8\eta_0\eta_0} - \sin 2\theta_{ps} g_{\sigma_8\eta_0\eta_8} + \cos^2\theta_{ps} g_{\sigma_8\eta_8\eta_8}\right), \end{aligned} \tag{B29}$$

$$\begin{aligned} g_{f_0\eta\eta} =& -\sin\theta_s \left(\sin^2\theta_{ps} g_{\sigma_0\eta_0\eta_0} - \sin 2\theta_{ps} g_{\sigma_0\eta_0\eta_8} + \cos^2\theta_{ps} g_{\sigma_0\eta_8\eta_8}\right) \\ &+ \cos\theta_s \left(\sin^2\theta_{ps} g_{\sigma_8\eta_0\eta_0} + \sin 2\theta_{ps} g_{\sigma_8\eta_0\eta_8} + \cos^2\theta_{ps} g_{\sigma_8\eta_8\eta_8}\right), \end{aligned} \tag{B30}$$

$$\begin{aligned} g_{\sigma\eta\eta'} =& \cos\theta_s \left(-\frac{\sin 2\theta_{ps}}{2} g_{\sigma_0\eta_0\eta_0} + \cos 2\theta_{ps} g_{\sigma_0\eta_0\eta_8} + \frac{\sin 2\theta_{ps}}{2} g_{\sigma_0\eta_8\eta_8}\right) \\ &+ \sin\theta_s \left(-\frac{\sin 2\theta_{ps}}{2} g_{\sigma_8\eta_0\eta_0} + \cos 2\theta_{ps} g_{\sigma_8\eta_0\eta_8} + \frac{\sin 2\theta_{ps}}{2} g_{\sigma_8\eta_8\eta_8}\right), \end{aligned} \tag{B31}$$

$$\begin{aligned} g_{f_0\eta\eta'} =& -\sin\theta_s \left(-\frac{\sin 2\theta_{ps}}{2} g_{\sigma_0\eta_0\eta_0} + \cos 2\theta_{ps} g_{\sigma_0\eta_0\eta_8} + \frac{\sin 2\theta_{ps}}{2} g_{\sigma_0\eta_0\eta_8}\right) \\ &+ \cos\theta_s \left(-\frac{\sin 2\theta_{ps}}{2} g_{\sigma_8\eta_0\eta_0} + \cos 2\theta_{ps} g_{\sigma_8\eta_0\eta_8} + \frac{\sin 2\theta_{ps}}{2} g_{\sigma_8\eta_0\eta_8}\right), \end{aligned} \tag{B32}$$

$$g_{a_0^\pm\pi^\mp\eta} = -\sin\theta_{ps} g_{a_0^\pm\pi^\mp\eta_0} + \cos\theta_{ps} g_{a_0^\pm\pi^\mp\eta_8}, \tag{B33}$$

$$g_{a_0^\pm\pi^\mp\eta'} = \cos\theta_{ps} g_{a_0^\pm\pi^\mp\eta_0} + \sin\theta_{ps} g_{a_0^\pm\pi^\mp\eta_8}, \tag{B34}$$

$$g_{a_0^0\pi^0\eta} = g_{\sigma_3\pi_3\eta} = -\sin\theta_{ps} g_{\sigma_3\eta_0\pi_3} + \cos\theta_{ps} g_{\sigma_3\pi_3\eta_8} \tag{B35}$$

The couplings that emerge from ISB are given as follows:

$$\begin{aligned} g_{a_0\pi^0\pi^0} =& g_{\sigma_3\pi_3\pi_3} + (\sin\theta_{\sigma_3\sigma}) g_{\sigma\pi_3\pi_3} + (\sin\theta_{\sigma_3 f_0}) g_{f_0\pi_3\pi_3} \\ &+ 2\sin\theta_{\pi^0\eta}(-\sin\theta_{ps} g_{\sigma_3\eta_0\pi_3} + \cos\theta_{ps} g_{\sigma_3\pi_3\eta_8}) \\ &+ 2\sin\theta_{\pi^0\eta'}(\cos\theta_{ps} g_{\sigma_3\eta_0\pi_3} + \sin\theta_{ps} g_{\sigma_3\pi_3\eta_8}), \end{aligned} \tag{B36}$$

$$g_{a_0^0\pi^+\pi^-} = g_{\sigma_3\pi^+\pi^-} + \sin\theta_{\sigma_3\sigma} g_{\sigma\pi^+\pi^-} + \sin\theta_{\sigma_3 f_0} g_{f_0\pi^+\pi^-}, \tag{B37}$$

$$\begin{aligned} g_{a_0^\pm\pi^\mp\pi^0} =& g_{a_0^\pm\pi^\mp\pi_3} + \sin\theta_{\pi^0\eta}\left(-\sin\theta_{ps} g_{a_0^\pm\pi^\mp\eta_0} + \cos\theta_{ps} g_{a_0^\pm\pi^\mp\eta_8}\right) \\ &+ \sin\theta_{\pi^0\eta'}\left(\cos\theta_{ps} g_{a_0^\pm\pi^\mp\eta_0} + \sin\theta_{ps} g_{a_0^\pm\pi^\mp\eta_8}\right), \end{aligned} \tag{B38}$$

$$\begin{aligned} g_{\sigma\pi^0\eta} =& g_{\sigma\pi_3\eta} = \cos\theta_s(-\sin\theta_{ps} g_{\sigma_0\pi_3\eta_0} + \cos\theta_{ps} g_{\sigma_0\pi_3\eta_8}) \\ &+ \sin\theta_s(-\sin\theta_{ps} g_{\sigma_8\pi_3\eta_0} + \cos\theta_{ps} g_{\sigma_8\pi_3\eta_8}), \end{aligned} \tag{B39}$$

$$\begin{aligned} g_{f_0\pi^0\eta} =& g_{f_0\pi_3\eta} = -\sin\theta_s(-\sin\theta_{ps} g_{\sigma_0\pi_3\eta_0} + \cos\theta_{ps} g_{\sigma_0\pi_3\eta_8}) \\ &+ \cos\theta_s(-\sin\theta_{ps} g_{\sigma_8\pi_3\eta_0} + \cos\theta_{ps} g_{\sigma_8\pi_3\eta_8}). \end{aligned} \tag{B40}$$

B.2. Meson–nucleon coupling constants

The couplings between the meson and nucleon are given as follows:

$$g_{\sigma_0 N} = \frac{g}{\sqrt{3}}, \tag{B41}$$

$$g_{\sigma_3 N} = \frac{g}{\sqrt{2}}\tau_3, \tag{B42}$$

$$g_{a_0^\pm N} = g, \tag{B43}$$

$$g_{\sigma_8 N} = \frac{g}{\sqrt{6}}, \tag{B44}$$

$$g_{\eta_0 N} = \frac{g}{\sqrt{3}}\gamma_5, \tag{B45}$$

$$g_{\pi_3 N} = \frac{g}{\sqrt{2}}\gamma_5\tau_3, \tag{B46}$$

$$g_{\pi^\pm N} = g\gamma_5, \tag{B47}$$

$$g_{\eta_8 N} = \frac{g}{\sqrt{6}}\gamma_5, \tag{B48}$$

$$g_{\sigma N} = \cos\theta_s g_{\sigma_0 N} + \sin\theta_{ps} g_{\sigma_8 N}, \tag{B49}$$

$$g_{f_0 N} = -\sin\theta_s g_{\sigma_0 N} + \cos\theta_s g_{\sigma_8 N}, \tag{B50}$$

$$g_{\eta' N} = \cos\theta_{ps} g_{\eta_0 N} + \sin\theta_{ps} g_{\eta_8 N}, \tag{B51}$$

$$g_{\eta N} = -\sin\theta_{ps} g_{\eta_0 N} + \cos\theta_{ps} g_{\eta_8 N}. \tag{B52}$$

B.3. Scalar–2-pseudoscalar meson couplings

First, we evaluate $\Gamma_{(\alpha)}$ from diagram (α) in Fig. 3. We divide $\Gamma_{(\alpha)}$ into three parts: $\Gamma^{(1)}_{(\alpha)}$, $\Gamma^{(2)}_{(\alpha)}$, and $\Gamma^{(3)}_{(3)}$ come from the diagrams with the nuclear hole state between σ_f and π_1, π_1 and π_2, and π_2 and σ_f, respectively. $\Gamma^{(1)}_{(\alpha)}$ is evaluated as follows:

$$\begin{aligned}
i\Gamma^{(1)}_{\alpha}(\rho) =& -\mathrm{tr}\int\frac{d^4p}{(2\pi)^4}(-ig_{\sigma_f N})(-2\pi)(\not{\tilde{q}}+\not{p}+m_N)\delta((\tilde{q}+p)^2-m_N^2)\theta(p_0+\tilde{q}_0)\theta(k_f-|\vec{\tilde{q}}+\vec{p}|)\\
&\times(g_1\gamma_5)\frac{i(\not{p}+\not{k}_2+m_N)}{(p+k_1)^2-m_N^2}(g_2\gamma_5)\frac{i(\not{p}+m_N)}{p^2-m_N^2}\\
=& ig_{\sigma_f N}g_1g_2\mathrm{tr}\int\frac{d^4p}{(2\pi)^3}\frac{(\not{p}+m_N)(-\not{p}+\not{k}_1+m_N)(\not{p}-\not{\tilde{q}}+m_N)}{((p-k_1)^2-m_N^2)((p-\tilde{q})^2-m_N^2)}\theta(p_0)\delta(p^2-m_N^2)\theta(k_f-|\vec{p}|)\\
=& ig_{\sigma_f N}g_1g_2\mathrm{tr}\int\frac{d^4p}{(2\pi)^3}\frac{4m_N(2p_1\cdot k_1-k_1^2-k_1\cdot k_2)}{((p-k_1)^2-m_N^2)((p-\tilde{q})^2-m_N^2)}\frac{1}{2E_N(\vec{p})}\delta(p_0-E_N(\vec{p}))\theta(k_f-|\vec{p}|)\\
\sim& ig_{\sigma_f N}g_1g_2\frac{2m_NE_1-m_1^2-k_1\cdot k_2}{(2m_NE_1-m_1^2)(2m_N(E_1+E_2)-(k_1+k_2)^2)}\rho_{p(n)}\\
\sim& i\frac{g_{\sigma_f N}g_1g_2}{2m_N(E_1+E_2)}\rho_{p(n)}.
\end{aligned} \tag{B53}$$

The meson–nucleon couplings $g_{\sigma_f N}$ and g_i are given in Appendix B.2. Using the same approximations as the calculation of scalar meson self-energy performed in Appendix A, we take only the leading-order contribution with respect to k_f and the external momenta k_i regarding them as small compared with the other quantities. From the third to the fourth line, we use the approximation where $E_N(\vec{p})$ is taken as m_N. In much the same way as the above calculation, $\Gamma^{(2)}_{\alpha}(k_f)$ and $\Gamma^{(3)}_{\alpha}(k_f)$ are written as

$$\begin{aligned}
i\Gamma^{(2)}_{\alpha}(\rho) =& -\mathrm{tr}\int\frac{d^4p}{(2\pi)^4}(-ig_{\sigma_f N})\frac{i}{\not{\tilde{q}}+\not{p}-m_N}(g_1\gamma_5)(-2\pi)(\not{p}+\not{k}_2+m_N)\\
&\times\theta(p_0+k_{20})\delta((p+k_2)^2-m_N^2)\theta(k_f-|\vec{p}+\vec{k}_2|)(g_2\gamma_5)\frac{i}{\not{p}-m_N}
\end{aligned}$$

$$
\begin{aligned}
=&ig_{\sigma_f N}g_1g_2\mathrm{tr}\int\frac{d^4p}{(2\pi)^3}\frac{(\not p+\not k_1+m_N)(-\not p+m_N)(\not p-\not k_2+m_N)}{((p+k_1)^2-m_N^2)((p-k_2)^2-m_N^2)}\\
=&ig_{\sigma_f N}g_1g_2\int\frac{d^4p}{(2\pi)^3}\frac{-4m_Nk_1\cdot k_2}{(2p\cdot k_1+m_1^2)(-2p\cdot k_2+m_2^2)}\\
\sim&ig_{\sigma_f N}g_1g_2\frac{k_1\cdot k_2}{(2m_NE_1+m_1^2)(2m_NE_2-m_2^2)}\rho_{p(n)}\sim i\frac{g_{\sigma_f N}g_1g_2}{4m_N^2E_1E_2}(k_1\cdot k_2)\rho_{p(n)}. \quad \text{(B54)}
\end{aligned}
$$

and

$$
\begin{aligned}
i\Gamma_\alpha^{(3)}(\rho)=&-\mathrm{tr}\int\frac{d^4p}{(2\pi)^4}(-ig_{\sigma_f N})\frac{i}{\not q+\not p-m_N}g_1\gamma_5\frac{i}{\not p+\not k_2-m_N}g_2\gamma_5(-2\pi)(\not p+m_N)\\
&\times\delta(p^2-m_N^2)\theta(p_0)\theta(k_f-|\vec p|)\\
=&ig_{\sigma_f N}g_1g_2\int\frac{d^4p}{(2\pi)^3}\frac{\mathrm{tr}(\not p+\not{\tilde q}+m_N)(-\not p-\not k_2+m_N)(\not p+m_N)}{\left((p+\tilde q)^2-m_N^2\right)\left((p+k_2)^2-m_N^2\right)}\frac{1}{2E_N(\vec p)}\theta(p_0)\theta(k_f-|\vec p|)\\
=&ig_{\sigma_f N}g_1g_2\int\frac{d^4p}{(2\pi)^3}\frac{-4m_N(2p+\tilde q)\cdot k_2}{\left((p+\tilde q)^2-m_N^2\right)\left((p+k_2)^2-m_N^2\right)}\frac{1}{2E_N(\vec p)}\theta(p_0)\theta(k_f-|\vec p|)\\
=&ig_{\sigma_f N}g_1g_2\int\frac{d^4p}{(2\pi)^3}\frac{-4m_N(2p+k_1+k_2)\cdot k_2}{(2p\cdot(k_1+k_2)+(k_1+k_2)^2)\left(2p\cdot k_2+k_2^2\right)}\frac{1}{2E_N(\vec p)}\theta(p_0)\theta(k_f-|\vec p|)\\
\sim&-ig_{\sigma_f N}g_1g_2\frac{2m_NE_2+k_1\cdot k_2+m_{\pi_2}^2}{(2m_N(E_1+E_2)+(k_1+k_2)^2)(2m_NE_2+m_{\pi_2}^2)}\rho_{p(n)}\\
\sim&-i\frac{g_{\sigma_f N}g_{\pi_1 N}g_{\pi_2 N}}{2m_N(E_1+E_2)}\rho_{p(n)}. \quad \text{(B55)}
\end{aligned}
$$

Thus, the correction of the couplings of mesons in the symmetric nuclear medium $i\Gamma_\alpha=i\Gamma_\alpha^{(1)}+i\Gamma_\alpha^{(2)}+i\Gamma_\alpha^{(3)}$ is given by

$$
i\Gamma_\alpha(\rho)=i\frac{g_{\sigma_f N}g_1g_2}{4m_N^2E_1E_2}(k_1\cdot k_2)\rho_{p(n)}. \quad \text{(B56)}
$$

B.4. 4-pseudoscalar meson vertex in the nuclear medium

Next, we evaluate diagram (β) in Fig. 3. We write $i\Gamma_\beta=i\Gamma_\beta^{(1)}+i\Gamma_\beta^{(2)}+i\Gamma_\beta^{(3)}+i\Gamma_\beta^{(4)}$. For $\Gamma_\beta^{(1)}$, the propagator between η and π_1 is the nuclear hole state. $\Gamma_\beta^{(1)}(q)$ is written as

$$
\begin{aligned}
i\Gamma_\beta^{(1)}(q)=&-\mathrm{tr}\int\frac{d^4p}{(2\pi)^4}(g_{\eta N}\gamma_5)(-2\pi)(\not p+\not q+m_N)\delta((p+q)^2-m_N^2)\theta(k_f-|\vec p+\vec q|)(g_1\gamma_5)\\
&\times\frac{i(\not p+\not k_2+\not k_3+m_N)}{(p+k_2+k_3)^2-m_N^2}(g_2\gamma_5)\frac{i(\not p+\not k_3+m_N)}{(p+k_3)^2-m_N^2}(g_3\gamma_5)\frac{i(\not p+m_N)}{p^2-m_N^2}\\
=&-ig_{\eta N}g_1g_2g_3\mathrm{tr}\int\frac{d^3p}{(2\pi)^3}\frac{(-\not p-\not q+m_N)(\not p+\not k_2+\not k_3+m_N)(-\not p-\not k_3+m_N)(\not p+m_N)}{((p+k_2+k_3)^2-m_N^2)((p+k_3)^2-m_N^2)(p^2-m_N^2)}\\
&\times\delta((p+q)^2-m_N^2)\theta(p_0+q_0)\theta(k_f-|\vec p+\vec q|)\\
=&-ig_{\eta N}g_1g_2g_3\mathrm{tr}\int\frac{d^4p}{(2\pi)^3}\frac{(-\not p+m_N)(\not p-\not k_1+m_N)(-\not p+\not k_1+\not k_2+m_N)(\not p-\not q+m_N)}{[(p-k_1)^2-m_N^2][(p-k_1-k_2)^2-m_N^2][(p-q)^2-m_N^2]}\theta(p_0)\\
&\times\delta(p^2-m_N^2)\theta(k_f-|\vec p|)\\
\sim&ig_1g_2g_3g_4\frac{2m_NE_1-k_1\cdot(k_1+k_2)}{(2m_NE_1-m_1^2)(2m_N(E_1+E_2)-(k_1+k_2)^2)(2m_N-m_\eta)}\rho_{p(n)}
\end{aligned}
$$

$$\sim i\frac{g_{\eta N}g_1g_2g_3}{4m_N^2(E_1+E_2)}\rho_{p(n)}. \tag{B57}$$

Here, the approximation taking $E_N(\vec{p})$ as m_N is used as in the case of the above calculation. $\Gamma_\beta^{(2)}(q)$, which is the contribution from the diagram with the nuclear hole state between π_1 and π_2, is evaluated as

$$\begin{aligned}
i\Gamma_\beta^{(2)}(q) =& -\mathrm{tr}\int\frac{d^4p}{(2\pi)^4}(g_{\eta N}\gamma_5)\frac{i(\not{p}+\not{q}+m_N)}{(p+q)^2-m_N^2}(g_1\gamma_5)(-2\pi)(\not{p}+\not{k}_2+\not{k}_3+m_N)\delta((p+k_2+k_3)^2-m_N^2)\\
&\times\theta(p_0+k_{20}+k_{30})\theta(k_f-|\vec{p}+\vec{k}_2+\vec{k_3}|)(g_2\gamma_5)\frac{i(\not{p}+\not{k}_3+m_N)}{(p+k_3)^2-m_N^2}(g_3\gamma_5)\frac{i(\not{p}+m_N)}{p^2-m_N^2}\\
=& -ig_{\eta N}g_1g_2g_3\mathrm{tr}\int\frac{d^4p}{(2\pi)^3}\frac{-\not{p}-\not{k}_1+m_N}{(p+k_1)^2-m_N^2}(\not{p}+m_N)\delta(p^2-m_N^2)\theta(p_0)\theta(k_f-|\vec{p}|)\\
&\times\frac{-\not{p}+\not{k}_2+m_N}{(p-k_2)^2-m_N^2}\frac{\not{p}-\not{k}_2-\not{k}_3+m_N}{(p-k_2-k_3)^2-m_N^2}\\
\sim& ig_{\eta N}g_1g_2g_3\frac{2m_NE_1E_2-E_1k_2\cdot(k_2+k_3)-E_2(k_1\cdot k_3)+E_3(k_1\cdot k_2)}{(2m_NE_1+m_1^2)(2m_NE_2-m_2^2)(2m_N(E_2+E_3)-(k_2+k_3)^2)}\rho_{p(n)}\\
\sim& i\frac{g_{\eta N}g_1g_2g_3}{4m_N^2(E_2+E_3)}\rho_{p(n)}.
\end{aligned} \tag{B58}$$

$\Gamma_\beta^{(3)}(q)$ with the hole state between π_2 and π_3 is given by

$$\begin{aligned}
i\Gamma_\beta^{(3)}(q) =& -\mathrm{tr}\int\frac{d^4p}{(2\pi)^4}(g_{\eta N}\gamma_5)\frac{i(\not{p}+\not{q}+m_N)}{(p+q)^2-m_N^2}(g_1\gamma_5)\frac{i(\not{p}+\not{k}_2+\not{k}_3+m_N)}{(p+k_2+k_3)^2-m_N^2}(g_2\gamma_5)(-2\pi)\\
&\times(\not{p}+\not{k}_3+m_N)\delta((p+k_3)^2-m_N^2)\theta(p_0+k_{30})\theta(k_f-|\vec{p}+\vec{k}_3|)(g_3\gamma_5)\frac{i(\not{p}+m_N)}{p^2-m_N^2}\\
=& -ig_{\eta N}g_1g_2g_3\mathrm{tr}\int\frac{d^4p}{(2\pi)^3}\frac{-\not{p}-\not{k}_1-\not{k}_2+m_N}{(p+k_1+k_2)^2-m_N^2}\frac{\not{p}+\not{k}_2+m_N}{(p+k_2)^2-m_N^2}(-\not{p}+m_N)\\
&\times\delta(p^2-m_N^2)\theta(p_0)\theta(k_f-|\vec{p}|)\frac{\not{p}-\not{k}_3+m_N}{(p-k_3)^2-m_N^2}\\
\sim& -ig_{\eta N}g_1g_2g_3\frac{2m_NE_2E_3-E_1(k_2\cdot k_3)+E_2(k_1\cdot k_3)+E_3k_2\cdot(k_1+k_2)}{[2m_N(E_1+E_2)+(k_1+k_2)^2][2m_NE_2+m_2^2][2m_NE_3-m_3^2]}\\
\sim& -i\frac{g_{\eta N}g_1g_2g_3}{4m_N^2(E_1+E_2)}\rho_{p(n)}.
\end{aligned} \tag{B59}$$

Finally, $i\Gamma_\beta^{(4)}(q)$, which is the contribution from the diagram with the hole state between π_3 and η, is written as

$$\begin{aligned}
i\Gamma_\beta^{(4)}(q) =& -\mathrm{tr}\int\frac{d^4p}{(2\pi)^4}(g_{\eta N}\gamma_5)\frac{i(\not{p}+\not{q}+m_N)}{(p+q)^2-m_N^2}(g_1\gamma_5)\frac{i(\not{p}+\not{k}_2+\not{k}_3+m_N)}{(p+k_2+k_3)^2-m_N^2}(g_2\gamma_5)\frac{i(\not{p}+\not{k}_3+m_N)}{(p+k_3)^2-m_N^2}\\
&\times(g_3\gamma_5)(-2\pi)(\not{p}+m_N)\delta(p^2-m_N^2)\theta(p_0)\theta(k_f-|\vec{p}|)\\
=& -ig_{\eta N}g_1g_2g_3\mathrm{tr}\int\frac{d^4p}{(2\pi)^3}\frac{-\not{p}-\not{q}+m_N}{(p+q)^2-m_N^2}\frac{\not{p}+\not{k}_2+\not{k}_3+m_N}{(p+k_2+k_3)^2-m_N^2}\frac{-\not{p}-\not{k}_3+m_N}{(p+k_3)^2-m_N^2}\\
&\times(\not{p}+m_N)\delta(p^2-m_N^2)\theta(p_0)\theta(k_f-|\vec{p}|)\\
\sim& -ig_{\eta N}g_1g_2g_3\frac{2m_NE_3+k_3\cdot(k_2+k_3)}{(2m_N+m_\eta)(2m_N(E_2+E_3)+(k_2+k_3)^2)(2m_NE_3+m_3^2)}\rho_{p(n)}
\end{aligned}$$

$$\sim -i\frac{g_{\eta N}g_1g_2g_3}{4m_N^2(E_2+E_3)}\rho_{p(n)}. \tag{B60}$$

From the above calculations, $i\Gamma_\beta(q) = i\Gamma_\beta^{(1)} + i\Gamma_\beta^{(2)} + i\Gamma_\beta^{(3)} + i\Gamma_\beta^{(4)}$ vanishes in this calculation.

C. Nucleon self-energy in the nuclear medium

We evaluate the contribution from the diagram in Fig. 4 to the self-energy Σ_N of the nucleon in the nuclear medium, which reads

$$\begin{aligned}
-i\Sigma_N =& \int \frac{d^4p}{(2\pi)^4}(-ig_{\sigma_f N})(-2\pi)(\not{p}+\not{q}+m_N)\theta(p_0+q_0)\delta((p+q)^2-m_N^2) \\
&\times \theta(k_f-|\vec{p}+\vec{q}|)(-ig_{\sigma_f N})\frac{i}{p^2-m_{\sigma_f}^2} \\
=& ig_{\sigma_f N}^2\int\frac{d^4p}{(2\pi)^3}(\not{p}+m_N)\theta(p_0)\delta(p^2-m_N^2)\theta(k_f-|\vec{p}|)\frac{1}{(p-q)^2-m_N^2} \\
=& ig_{\sigma_f N}^2\int\frac{d^3p}{(2\pi)^3}(\not{p}+m_N)\frac{1}{2E_N(\vec{p})}\frac{1}{2m_N^2-2m_NE_N(\vec{p})-m_{\sigma_f}^2}\bigg|_{p_0=E_N(\vec{p})}.
\end{aligned}$$

Setting the incoming nucleon momentum as $q=(m_N,\vec{0})$ and ignoring the higher-order terms with respect to k_f, Σ_N is obtained as

$$-i\Sigma_N = ig_{\sigma_f N}^2\int\frac{d^3p}{(2\pi)^3}(2m_N)\frac{1}{2m_N}\frac{1}{-m_{\sigma_f}^2} \tag{C1}$$

$$= -i\frac{g_{\sigma_f N}^2}{2m_{\sigma_f}^2}\rho_{p(n)}. \tag{C2}$$

References

[1] D. Sutherland, Phys. Lett. **23**, 384 (1966).
[2] J. A. Cronin, Phys. Rev. **161**, 1483 (1967).
[3] J. S. Bell and D. Sutherland, Nucl. Phys. B **4**, 315 (1968).
[4] H. Osborn and D. Wallace, Nucl. Phys. B **20**, 23 (1970).
[5] R. Baur, J. Kambor, and D. Wyler, Nucl. Phys. B **460**, 127 (1996).
[6] C. Ditsche, B. Kubis, and U.-G. Meißner, Eur. Phys. Jour. C **60**, 83 (2009).
[7] J. Schechter and Y. Ueda, Phys. Rev. D **4**, 733 (1971).
[8] W. Hudnall and J. Schechter, Phys. Rev. D **9**, 2111 (1974).
[9] S. Weinberg, Phys. Rev. D **11**, 3583 (1975).
[10] J. Kogut and L. Susskind, Phys. Rev. D **11**, 3594 (1975).
[11] S. Raby, Phys. Rev. D **13**, 2594 (1976).
[12] K. Kawarabayashi and N. Ohta, Nucl. Phys. B **175**, 477 (1980).
[13] H. Leutwyler, Phys. Lett. B **374**, 181 (1996).
[14] A. H. Rosenfeld et al., Rev. Mod. Phys. **36**, 977 (1964).
[15] G. Salvini.
[16] A. Neveu and J. Scherk, Ann. Phys. **57**, 39 (1970).
[17] C. Roiesnel and T. N. Truong, Nucl. Phys. B **187**, 293 (1981).
[18] J. Gasser and H. Leutwyler, Nucl. Phys. B **250**, 539 (1985).
[19] J. Kambor, C. Wiesendanger, and D. Wyler, Nucl. Phys. B **465**, 215 (1996).
[20] A. V. Anisovich and H. Leutwyler, Phys. Lett. B **375**, 335 (1996).
[21] A. Abdel-Rehim, D. Black, A. H. Fariborz, and J. Schechter, Phys. Rev. D **67**, 054001 (2003).
[22] B. Borasoy and R. Nissler, Eur. Phys. Jour. A **26**, 383 (2005).
[23] J. Bijnens and K. Ghorbani.

[24] S. Lanz, PoS CD **12**, 007 (2013).
[25] P. Guo et al., Phys. Rev. **D92**, 054016 (2015).
[26] R. S. Hayano and T. Hatsuda, Rev. Mod. Phys. **82**, 2949 (2010).
[27] S. Sakai and T. Kunihiro.
[28] D. Jido, T. Hatsuda, and T. Kunihiro, Phys. Rev. D **63**, 011901 (2000).
[29] T. Hatsuda, T. Kunihiro, and H. Shimizu, Phys. Rev. Lett. **82**, 2840 (1999).
[30] K. A. Olive et al., Chin. Phys. **C38**, 090001 (2014).
[31] J. A. Oller and E. Oset.
[32] R. Jaffe, Phys. Rev. D **15**, 267 (1977).
[33] H. Gomm, P. Jain, R. Johnson, and J. Schechter, Phys. Rev. D **33**, 801 (1986).
[34] Y. Nambu and G. Jona-Lasinio, Phys. Rev. **122**, 345 (1961).
[35] Y. Nambu and G. Jona-Lasinio, Phys. Rev. **124**, 246 (1961).
[36] T. Hatsuda and T. Kunihiro, Phys. Rept. **247**, 221 (1994).
[37] T. Hatsuda and T. Kunihiro, Prog. Theor. Phys. **74**, 765 (1985).
[38] T. Hatsuda and T. Kunihiro, Phys. Rev. Lett. **55**, 158 (1985).
[39] V. Bernard, U. G. Meissner, and I. Zahed, Phys. Rev. Lett. **59**, 966 (1987).
[40] T. Kunihiro, Prog. Theor. Phys. Suppl. **120**, 75 (1995).
[41] G. E. Brown and M. Rho, Phys. Rept. **269**, 333 (1996).
[42] R. Rapp and J. Wambach, Adv. Nucl. Phys. **25**, 1 (2000).
[43] N. Kelkar, K. Khemchandani, N. Upadhyay, and B. Jain, Rep. Prog. Phys. **76**, 066301 (2013).
[44] S. Sakai and D. Jido, Phys. Rev. C **88**, 064906 (2013).
[45] R. Dashen, Phys. Rev. **183**, 1245 (1969).
[46] K. Suzuki et al., Phys. Rev. Lett. **92**, 072302 (2004).